# Computational Modeling of Neurons Involved in Fly Motion Detection

by

Zuley Rivera Alvidrez

---

A Thesis Submitted to the Faculty of the

## Department of Electrical and Computer Engineering

In Partial Fulfillment of the Requirements
For the Degree of

## Masters of Science

In the Graduate College

## The University of Arizona

2 0 0 5

# Acknowledgements

I would like to thank my research advisor, Professor Charles Higgins, for giving me the freedom to choose the research directions that were most interesting to me, and for his encouragement and advice. I would like to thank Professor Nicholas Strausfeld and Dr. John Douglass for their encouragement and their willingness to answer my questions via email or via insightful discussions. I am thankful to Professor Sarma Vrudhula whose guidance and support has always been invaluable to me. I am grateful to my family and to Nathan Crockett for their unconditional love and understanding.

# Dedication

I would like to dedicate this thesis to my family. I am most grateful for their support, understanding and love through every step of my career.

# TABLE OF CONTENTS

# List of Figures

# ABSTRACT

Flying insects possess remarkable navigation abilities, and may be used as an inspiration for the design of fast, low-power, robust autonomous robots. Essential to visual insect navigation is complex motion detection circuitry. A neuronally-based model for elementary motion detectors (EMDs) in the fly has been previously proposed, but there are a number of computational features that are not supported by this model. We propose an expanded version of the model incorporating saturation and motion adaptation, and show simulation results that match recordings of the electrical activity of fly motion-sensitive interneurons. Our expanded model is used to explain data which suggests adaptation of the EMD filter parameters and the results of genetic experiments in which cells proposed to be involved in motion detection were successfully blocked in flies. In addition, we have identified a possible mechanism through which insects could extract speed information from the projected retinal image.

<div align="center">

Chapter 1

# Fly Motion Detection

</div>

## 1.1 Introduction

Flies have been around for over three hundred million years (for a review see Borst and Haag, 2002). With over 125,000 different fly species on the planet (Yeates and Wiegmann, 1999), they appear to be one of the most evolutionarily successful animals on Earth. From an engineering perspective, the fly's capabilities are remarkable. A fly with less than 10 $\mu$W of power and 100 mg of weight can achieve turning velocities of more than 3000 deg/sec and react with delay times less than 30 ms (Land and Collett, 1974; Wagner, 1986). Understanding the principles governing the neural processes in the fly could aid in the design of fast, low-power, robust autonomous robots.

Underlying the remarkable navigational capabilities of the fly is superb motion detection circuitry in its visual system. Motion detection is crucial for a number of important behaviors in flying insects, including visual tracking (Collett and Land, 1978; Egelhaaf *et al.*, 1988; Land, 1992; Lehrer and Srinivasan, 1992), gaze control (Hengstenberg, 1993), prey pursuit (Olberg *et al.*, 2000), and visual course control (for a review see Borst and Dickinson, 2003). Furthermore, it is also involved in range estimation for object avoidance (Kirchner and Srinivasan, 1989; Srinivasan *et al.*, 1991), and approach or landing (Braitenburg and Taddei, 1966; Wagner, 1982). The process of computing motion from the visual input may thus be key to the understanding of more complex insect behavior.

The main focus of this thesis is the study of motion detection in the fly. While there are different ways to approach this problem, we are interested in the development of neuronally-based models that reflect the types of computations that may be taking place in specific cells in the fly's visual system. A neuronally-based model that incorporates anatomical and electrophysiological data can be used to generate hypotheses about the properties of the specific neurons that it incorporates, which can then be used to guide future experiments and advance our understanding of this system.

A neuronally-based model of motion detection recently proposed by Higgins *et al.* (2004) and explained in Section 2.1 will be used as the substrate for the computational features that this thesis explores. While there are a number of aspects of motion detection that are not yet well understood, we chose to focus on the ones that have a value from an engineering perspective. Chapter 3 deals with contrast and pattern size saturation, Chapters 4 and 5 are devoted to the study of adaptation, Chapter 6 provides a study of redundancy and robustness in the network, and Chapter 7 explores a possible mechanism for a velocity detector. Final comments and future work are summarized in Chapter 8.

With the high volume of neuroscience content in this work, the reader will find that this is not a typical Electrical Engineering thesis. The reader may also agree that the current engineering or computer science approaches to traditionally difficult problems, such as computer vision or artificial intelligence, have been rather unsuccessful by many standards. Perhaps the only way we will achieve success is by taking advantage of the knowledge embedded in biological systems which have already solved these problems hundreds of millions of years of ago.

## 1.2 Motion Detection and the Fly's Visual System

Whenever a fly moves, the projection of the visual world on its retinae moves as well. The moving pattern, also called optic flow, is processed by the visual system and used by the fly to navigate in its environment. Motion originating from self-displacements and from moving objects in the fly's
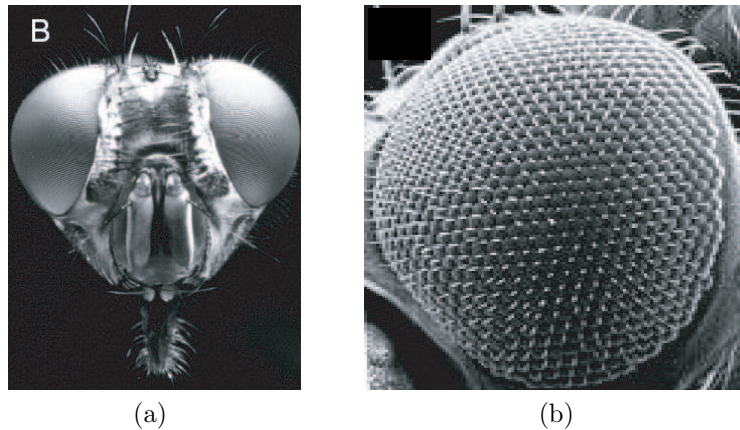
FIGURE 1.1. The eyes of a fly. (a) Front view of a female fly (*Calliphora vicina*). (b) Scanning Electron Microscope (SEM) image of the compound eye of a fly (*Drosophila Melanogaster*) showing the numerous facets. Panels **a** and **b** reproduced without permission from Gabriel (2004) and Fetchko (2002), respectively.

visual field is not an inherent property of the retinal image and must be computed by processing local changes in light intensity (for a review see Feng, 2003).

The eyes of a fly are composed of many individual facets called ommatidia (see Figure 1.1). Each eye has thousands of ommatidia, each of them accommodating eight photoreceptors referred to as R1 through R8 (Beersma *et al.*, 1977). The lens in each ommatidium focuses light onto the photoreceptors, which detect light through a chemical phototransduction process and send axons to a part of the fly's brain called the visual ganglia. The visual ganglia, shown in Figure 1.2, consist of four layers: the lamina, the medulla, the lobula and the lobula plate. Each of these layers is organized into repeated groups of cells which process information from the same visual unit. Each of these visual processing units is referred to as a *column* or *optic cartridge* and the cells comprising each column are referred to as *columnar elements*. In addition, adjacent columns in a layer correspond to adjacent points in the visual image. This type of organization is referred to as a *retinotopic* organization.

Photoreceptors R1-R6 are sensitive to UV or blue-green light, and are believed to be the input to elementary motion detectors (EMDs) which compute motion by comparing changes in light intensity from adjacent visual units. Because each of these EMDs processes information from only a small region of the fly's visual field, they are said to be *small-field* sensitive. EMDs are believed to be the input to visual interneurons in the fly's lobula plate, called lobula plate tangential cells (LPTCs). The receptive field of each LPTC covers a large area of the visual field, and are therefore said to be *wide-field* sensitive. There are about 60 different and uniquely identifiably LPTCs in each hemisphere (Hausen, 1982; Hengstenberg, 1983; Eckert and Dvorak, 1983). The large size of these cells facilitates electrophysiological recordings and numerous experiments with LPTC recordings have been documented. As a result, a lot of what is known about motion detection is based on LPTC experiments.

LPTCs are sensitive to motion in a directionally-selective and orientation-selective manner (for a review see Borst and Haag, 2002). Horizontal-system cells (called HS cells), two centrifugal cells (called CH cells) and cells H1 through H4 respond to horizontally-oriented motion. Three cells are included in the horizontal system and are named according to the region of the lobula plate where they extend their dendrites: HSN (northern region), HSE (equatorial region), and HSS (southern region). Similarly, there are two centrifugal cells per hemisphere, the dorsal dCH cell and the ventral
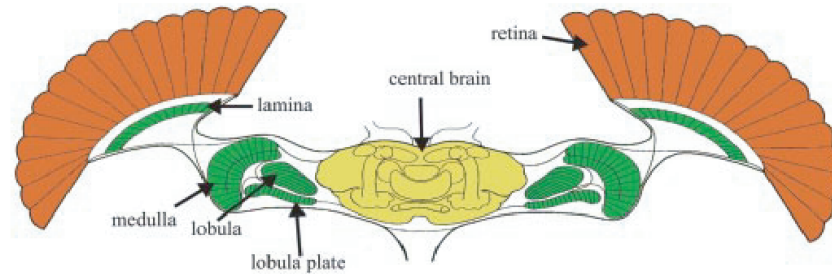
FIGURE 1.2. Schematic cross-section through the fly's head, showing the location of the retina and the layers of the visual ganglia: the lamina, medulla, lobula and lobula plate. Reproduced without permission from Borst and Haag (2002).
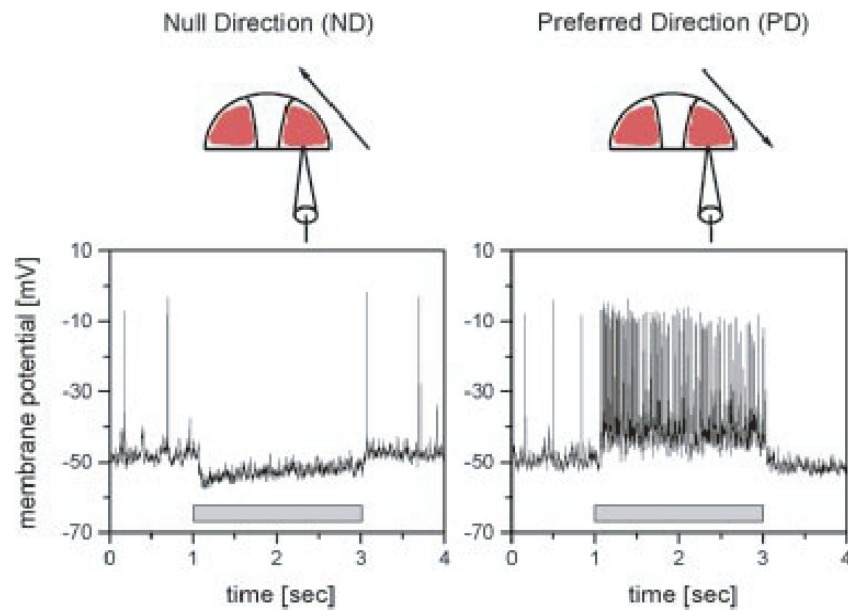


FIGURE 1.3. Intracellular recordings from an HSE tangential cell responding to motion stimuli in the cell's preferred and null directions. Reproduced without permission from Borst and Haag (2002).
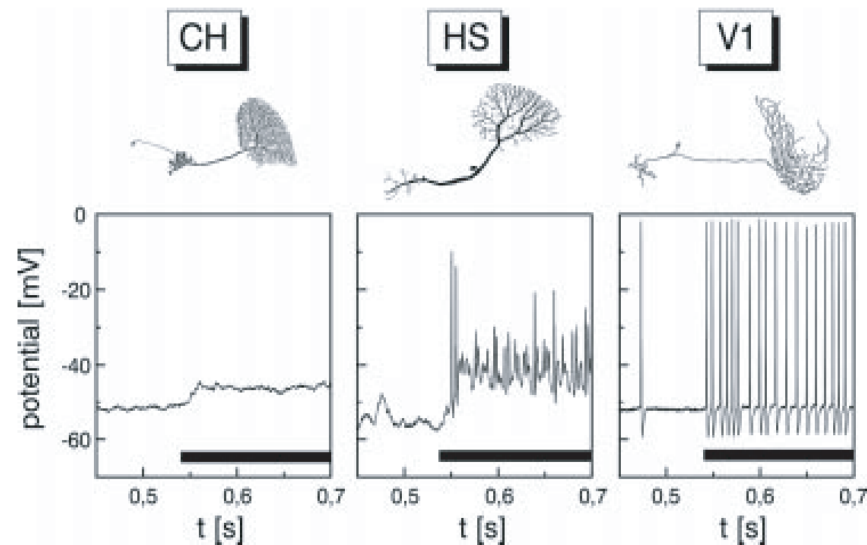
FIGURE 1.4. Lobula plate tangential cells. CH cells and HS cells are horizontally-sensitive. V1 cells are sensitive to motion oriented vertically. The response from CH cells is purely graded, the response of V1 cells is purely spiking, and the response of HS cells is a mixture of both. Reproduced without permission from Borst and Haag (2002).

vCH cell. Vertical-system cells (VS cells) and V1 cells respond to vertically-oriented motion. The vertical system includes the cells VS1 through VS11, which are numbered sequentially according to the region of the lobula plate where their dendrites are located. In addition, LPTCs are sensitive to the direction of moving visual stimuli and are excited (or depolarized) by motion in certain directions and inhibited (or hyperpolarized) by other directions of motion. The direction of motion that elicits the highest level of excitation in an LPTC is referred to the cell's *preferred direction* (PD), while the direction of motion that elicits the highest level of inhibition is referred to as the cell's *null direction* (ND), as illustrated in Figure 1.3. The *anti-preferred* direction is the direction of motion that points $180^o$ from the cell's preferred direction, and is not necessarily equal to the cell's null direction. Moreover, while some LPTCs respond with trains of action potentials (H1 through H4 and V1 cells), some respond with only graded shifts of membrane potentials (CH cells), and some with a mixture of both (HS and VS cells), as shown in Figure 1.4. LPTCs are important for flight control and are thought to be involved in the optomotor response (Hausen, 1984), a compensatory turn that the fly makes in response to large field rotations of the visual world due to unintended trajectory deviations.

## 1.3 Characterizing Motion Detection

Because sinusoidal and square-wave gratings provide a convenient way to characterize the temporal and spatial characteristics of the fly visual system, they have become the visual stimuli of choice in the study of motion detection. Traditionally, motion detection in the fly has been studied either by measuring the strength of the optomotor behavioral response or by recording the electrical activity of LPTCs as flies are shown moving patterns. Two examples of these experimental paradigms are
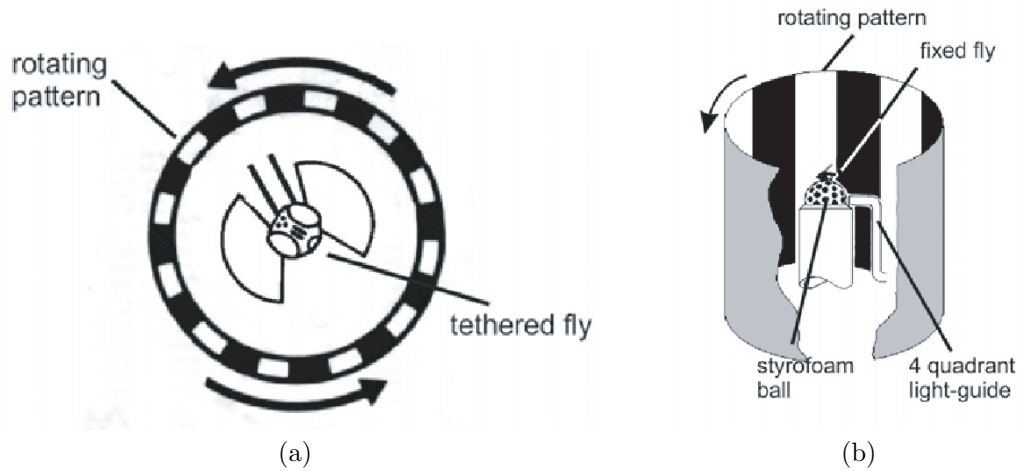
FIGURE 1.5. Experimental setups used to study fly motion-detection. (a) In some experiments immobilized flies were shown a moving square-wave pattern while recording from LPTCs (Dvorak *et al.*, 1979; Egelhaaf and Borst, 1989). (b) Experimental setup used to measure the optomotor response in walking, by computing the rotations of a floating styrofoam ball on which the flies walk as a wide-field grating moves around them (Keller, 2002). Both panels reproduced without permission from Keller (2002).

shown in Figure 1.5.

The study of the optomotor response led to the development of the Hassenstein-Reichardt (HR) model of motion detection (Hassenstein and Reichardt, 1956). This model has been shown to predict both the optomotor response characteristics and the responses of LPTCs (Egelhaaf *et al.*, 1988). The canonical version of this model is shown in Figure 1.6a. The computation of motion is based on the multiplication of a local photoreceptor signal with the delayed (low-pass filtered) signal from a neighboring photoreceptor. Figures 1.6b and 1.6c show other versions of the HR model with high-pass filters in all input pathways (Harris and O'Carroll, 2002) and with high-pass filters in two of the pathways (Borst *et al.*, 2003), respectively. The high-pass filters in the input paths prevent DC inputs from propagating forward, so only changes in light-intensity are transmitted.

It is widely believed that LPTCs combine the output of arrays of EMDs (Franceschini *et al.*, 1989; Egelhaaf *et al.*, 1989; Krapp *et al.*, 1998). The response of each EMD appears to also follow the type of response predicted by the HR model (Franceschini *et al.*, 1989). Figure 1.7 illustrates the view of LPTCs as spatial integrators of local HR models, representing individual EMDs. A limitation of the HR model is that it does not provide any insight into how this type of computation may be neuronally implemented. This becomes especially important when trying to characterize more complicated systems, such as the prey-pursuit system, which receives input from cells believed to be in the motion-detection pathway (Gronenberg and Strausfeld, 1991). Since the inputs to LPTCs are columnar elements, it follows that the cells implementing each EMD would be located in the columns of the layers of the visual ganglia. The possible identity of these cells is the subject of the next chapter.
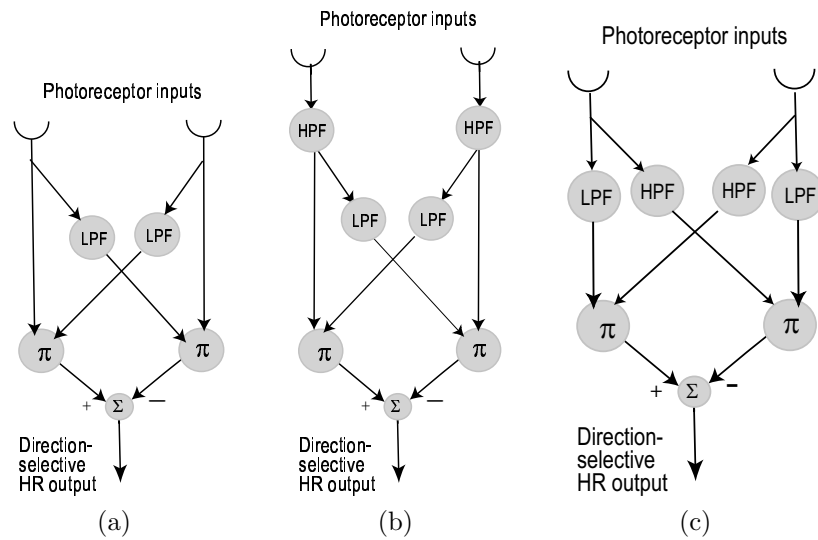
FIGURE 1.6. The Hassenstein-Reichardt (HR) model. (a) In this canonical HR model, the input from a photoreceptor is multiplied by the delayed (low-pass filtered) signal from the neighboring input unit. The computation of the difference between the two multiplications results in a directionally-selective output. LPF is a low-pass filter, $\sum$ and $\prod$ represent sum and multiplication. (b) A second version of the HR model with high-pass filtered (HPF) input pathways. (c) A third version of the HR model with high-pass filters in two of the pathways and low-pass filters in the other two.
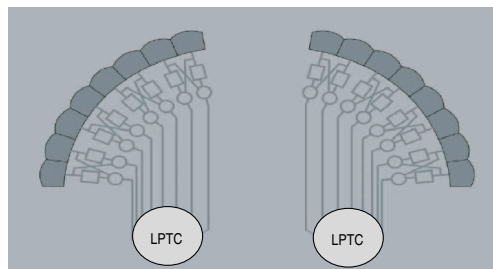


FIGURE 1.7. LPTCs are believed to combine the outputs of elementary motion detectors, the responses of which can be modeled by local HR models. Panel was modified from Feng (2003).

Chapter 2

# Neuronally-Based Models of Motion Detection

While the Hassenstein-Reichardt model of motion detection has been widely used since the 1950's, it does not provide any insight into the neuronal implementation of this computation. Unlike the HR model, a neuronally-based model may serve as a substrate for the understanding of the neural basis of motion detection and can be used to derive testable hypotheses about the network of cells and synapses that it represents.

## 2.1   The Neuronally-Based EMD Model

Using comparative studies among different fly species, a subset of the more than 40 columnar elements have been found to be ubiquitously conserved and have been proposed to be involved in motion detection (Buschbeck and Strausfeld, 1996). Recently, a model of elementary motion detection incorporating these neurons was shown to be as successful as the Hassenstein-Reichardt model in predicting the responses of tangential cells to a variety of visual stimuli (Higgins *et al.*, 2004). The mathematical relationships between the network of cells in the model are based on anatomical, electrophysiological, and histological studies.

The neuronal circuit, shown in Figure 2.1, includes lamina amacrine cells, lamina monopolar cells, the basket T-cell T1, the transmedullary cells Tm1 and Tm9, the T5 bushy T-cell, and an inhibitory interneuron. The foundations of the model are detailed elsewhere (Higgins *et al.*, 2004). Briefly, amacrine cells receive photoreceptor input and have been shown to synapse onto the T1 basket T-cell (Campos-Ortega and Strausfeld, 1973). Because T1 shows an inverted response to that of the photoreceptors and has a small DC component (Douglass and Strausfeld, 2004), the signal from the amacrine cell in the model is sign-inverted and filtered with a relaxed high-pass filter containing a small low-pass component (to allow for a small DC signal to be transmitted to T1). The lamina monopolar cell L2, also receiving photoreceptor input, is modeled with a sign-inverted high-pass filter, as no sustained component has been detected in the L2 cell response (Coombe *et al.*, 1989). Both L2 and T1 are presynaptic to Tm1 (Campos-Ortega and Strausfeld, 1973), but while L2 receives input from the photoreceptor in the same optic cartridge, T1 carries signals from amacrine cell processes expanding to neighboring units. One dimensional and two dimensional versions of the model have been proposed, differing only in the way that T1 is computed. In the one dimensional model, T1 is computed by adding low-pass filtered amacrine signals from two neighboring photoreceptors, as shown in Fig. 2.1. In the two-dimensional model, low-pass filtered amacrine signals from a hexagonal array of neighboring photoreceptors are added at T1. The response of the transmedullary cell Tm1 is computed by adding T1 and the local signal from L2. Tm1 responds to motion in any orientation and because it receives both a local input and the delayed (low-pass filtered) signals from neighboring visual units, it is a candidate for encoding *non-directional motion* in its amplitude. This would imply that the cell is more sensitive to motion than to flicker, but unlike a directionally-selective cell, it is unable to distinguish between motion in different directions.

While histological studies suggest a role for Tm1 as an excitatory input to the T5 cell, a second transmedullary cell, Tm9, is likely an inhibitory synaptic input (Snakevitch and Strausfeld, 2004). In addition, the processes of Tm1 coincide with Tm9. Both Tm1 and Tm9 terminate at the level of T5, but the Tm9 unit is displaced one visual sampling unit. The interaction of these three cells is modeled as a Barlow-Levick motion detector (Barlow and Levick, 1965), which computes
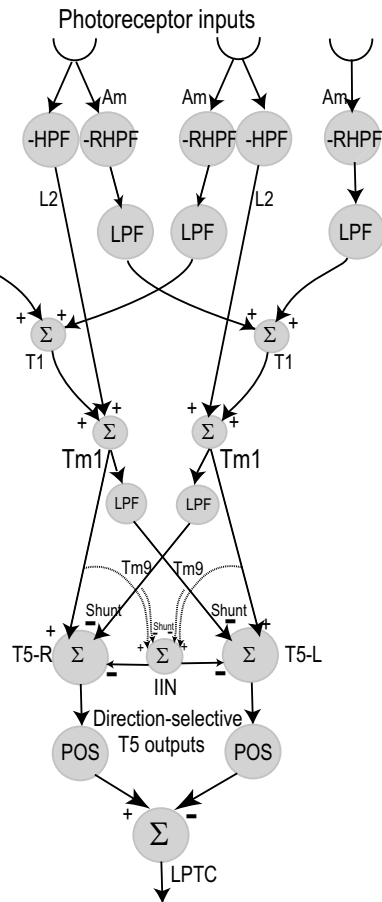
FIGURE 2.1. The one-dimensional neuronally-based model of elementary motion detection incorporating amacrine cells (Am), lamina monopolar cells (L2), basket T-cells (T1), two types of transmedullary cells (Tm1 and Tm9), T5 bushy T-cells (T5-R and T5-L) and an inhibitory interneuron (IIN). Excitatory and inhibitory inputs are represented by arrows with positive and negative signs, respectively. RHPF (relaxed high-pass filter) represents a HPF with a small low-pass component. A filter preceded by a negative sign indicates that the output of the filter was sign-inverted. Inhibitory inputs from the Tm9 cell are implemented as shunting. The inputs from T5 are rectified (POS) and subtracted by the tangential cell model. Note that the diagram does not necessarily represent individual cells, but rather the mathematical relationships between the various cell responses.

motion through the interaction of an excitatory input (Tm1) with a delayed inhibitory input from a neighboring unit (Tm9). The inhibition from Tm9 is shunting (a nonlinear inhibition, see Section 2.3), producing the nonlinearity required for directional selectivity. Full directional selectivity at the level of T5 is achieved through an inhibitory interneuron. In order to reproduce data from Borst *et al.* (1997), the T5 inputs to the tangential cell are rectified and subtracted (see Melano and Higgins (2005) for details).

## 2.2    An Expanded Model

While the neuronally-based model described in the previous section is able to predict the rough response of LPTCs in a variety of experiments, there are a number of features of the tangential cell response that are not captured by the neuronally-based model or by the Hassenstein-Reichardt model previously introduced. Our work for this thesis consisted of the incorporation of these features in an expanded neuronally-based model, which is shown in Figure 2.2. Just as with the original neuronally-based model, one dimensional and two dimensional versions of the model are possible depending on how T1 is computed (see Section 2.1). The features incorporated include contrast saturation and gain control (Chapter 3) and adaptation (Chapters 4). Moreover, the expanded model is used in this thesis to explain and provide insight into the results of a number of experiments, including impulse response data previously explained in terms of EMD filter adaptation (Chapter 5) and the results of genetic experiments in which specific cells from the proposed motion detection pathway were successfully blocked in flies (Chapter 6). In addition, the expanded model is used to explore a possible mechanism for speed estimation (Chapter 7).

## 2.3    Modeling and Simulation Methods

All simulations were run using the *Matlab* software (The Mathworks, Natick, MA). The two-dimensional simulations incorporated a $100 \times 10$ pixel image viewed by a $50 \times 5$ hexagonal array of photoreceptors and an equal number of EMD models. Unless otherwise specified, the simulations were as follows. The two-dimensional model was used with filters implemented as first order with time constants of 250 ms for the high pass filters, 150 ms for the first low-pass and 50 ms for the final low-pass filters. The time-step used for all simulations was 10 ms. Shunting inhibition was modeled as a "dirty multiplication" (Koch, 1999):

$$F(I_e, I_s) = pos(I_e) \cdot (1 - \frac{pos(I_s)}{I_{smax}}) \tag{2.1}$$

where the function $pos()$ indicates that negative quantities are set to zero, $I_e$ and $I_s$ represent excitatory and shunting inputs respectively, and $I_{smax}$ is the maximum possible value of $I_s$.

A two-dimensional sinusoidal grating moving in the horizontal direction was used as visual stimulus

$$I(x, y, t) = \frac{1}{2} \cdot (1 + C \cdot sin(\omega_t \cdot t + \omega_x \cdot x + \omega_y \cdot y + \phi)) \tag{2.2}$$

where $t$ represents time, $x$ and $y$ are the spatial dimensions, $C$ is contrast, $\omega_t$ is the temporal frequency, $\omega_x$ and $\omega_y$ are the spatial frequencies and $\phi$ is the phase. The inputs to the simulated tangential cell were rectified T5 outputs as described in Melano and Higgins (2005).
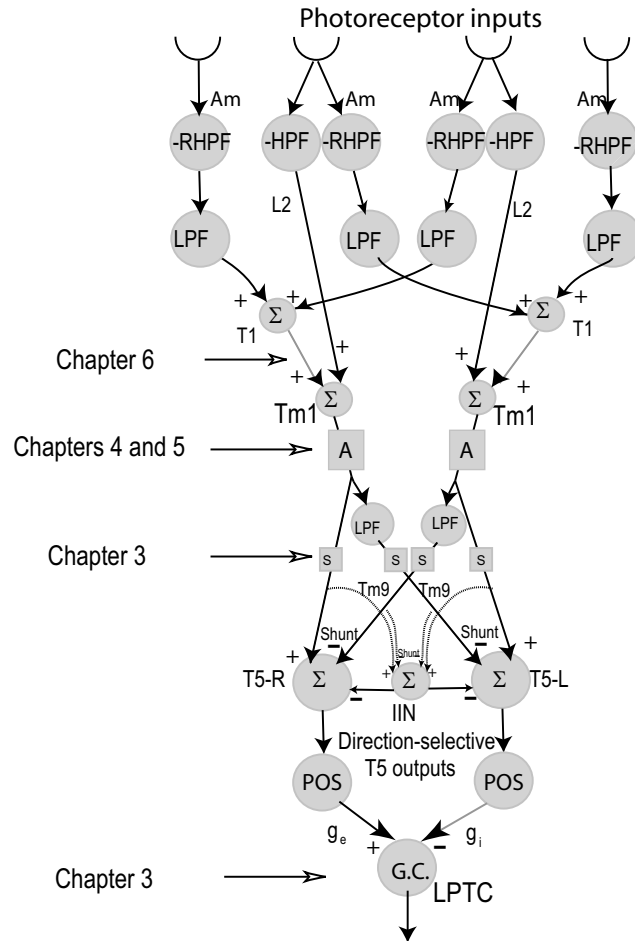
FIGURE 2.2. The one-dimensional version of the expanded neuronally-based model of elementary motion detection. The changes made to the model are explained in subsequent chapters. Chapter 3 describes the integration of a saturating nonlinearity ('S' blocks) into the T5 inputs and the incorporation of pattern size saturation, also called gain control (G.C.), into the computation of the simulated LPTC response. Chapters 4 and 5 discuss adaptation, which is proposed to occur in the Tm1 synapses ('A' blocks). The relative contributions of T1 and L2 to the model response are discussed in Chapter 6.

# CONTRAST AND PATTERN SIZE SATURATION

The response of a tangential cell increases with increasing stimulus contrast before reaching a constant level. This saturating response may be important for providing the cell with an estimate of the stimulus temporal frequency irrespective of its contrast (Egelhaaf and Borst, 1989). A similar type of response is produced when the size of the stimulus is increased. Saturation with pattern size makes the response of the cell insensitive to sparseness or gaps in the moving visual field or optic flow (Borst *et al.*, 1995). In this chapter, we show how both types of saturation may be incorporated in the expanded neuronally-based model. The model results in contrast sensitivity functions that compare favorably with tangential cell recordings. The results provide additional evidence in support of the model while allowing new insights into the nature of contrast saturation.

## 3.1  Background and Previous work

The responses of both the neuronally-based EMD model and the HR model (Hassenstein and Reichardt, 1956) as presented in Figure 2.1 and Figure 1.6, respectively, increase as the square of the contrast of the visual input. In biology, such an increase could only be sustained at very low visual contrasts, beyond which tangential cells have been shown to saturate (see Fig. 3.1a). Egelhaaf *et al.* (1989) successfully modeled this behavior by inserting a saturating nonlinearity into the canonical HR model shown in Fig. 1.6a. Unfortunately, the modified HR model provides little insight into where in the motion detection pathway of the insect this saturation could arise.

A second type of saturation in a tangential cell response occurs as the size of the visual stimulus is increased. This saturation makes the response of the cell insensitive to gaps or sparseness in the optic flow at sufficiently large sizes of pattern stimulus. Furthermore, the saturation level reached by the cell depends on the stimulus parameters, specifically on the speed of the stimulus (see Fig. 3.1b). The mechanisms through which the cell achieves this gain control are well understood (Borst *et al.*, 1995, 1997) and involve the biophysics of the membrane potential. EMDs responding in the cell's preferred direction are modeled as excitatory synaptic inputs, while EMDs responding in the null direction are inhibitory (see Methods). In this chapter we show that pattern size saturation can be modeled by incorporating these changes into the way that an array of neuronally-based EMD models (refer to Fig. 2.2) are combined to produce the simulated LPTC response.

## 3.2  Methods

Contrast saturation was implemented using a sigmoid function:

$$S(x) = C_1 + C_2 \cdot \frac{1}{1 + e^{-C_3 \cdot x}} \tag{3.1}$$

with parameters $C_1 = -.085$, $C_2 = .17$ and $C_3 = 43$ set to match the electrophysiological data (refer to Fig. 3.1a) at transient and steady-state conditions. This saturating nonlinearity was inserted in the blocks labeled 'S' in the diagram shown in Figure 2.2.

LPTC integration of EMD inputs (also called "gain control") was implemented as described in Borst *et al.* (1995, 1997) to produce pattern size saturation, using:

$$V = \frac{E_e g_e + E_i g_i}{g_e + g_i + g_{leak}} \tag{3.2}$$
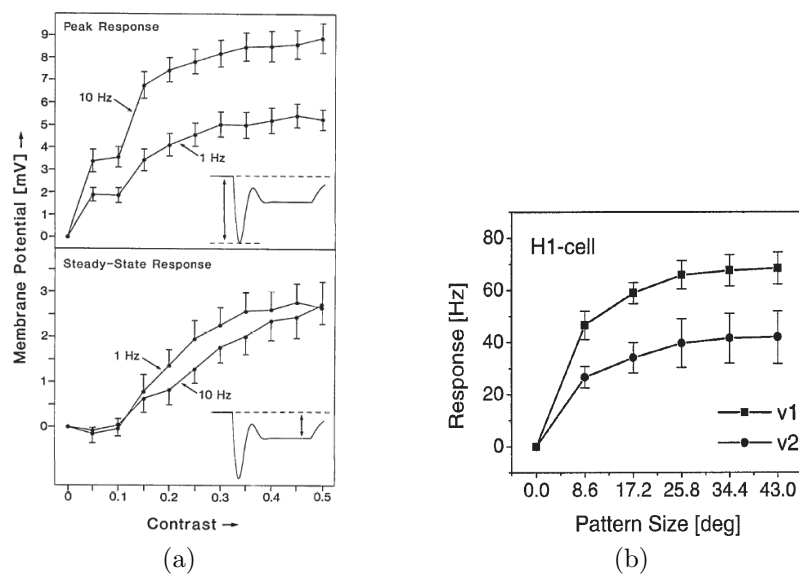
FIGURE 3.1. Saturation in LPTC responses. (a) Peak and steady-state responses from HS tangential cells for stimuli moving in the null direction at two temporal frequencies: 1 and 10 Hz. Peak responses were computed as the maximum response amplitude reached at the onset of motion (see inset in top plot), while steady-state responses were computed as the mean value after the response had become stable (see inset in bottom plot). (b) Mean response of an H1 cell as the size of a stimulus pattern is increased for two stimulus velocities: v1 = 72 deg/sec and v2 = 360 deg/sec. Panels **a** and **b** are reproduced without permission from Egelhaaf and Borst (1989) and Borst *et al.* (1997), respectively.

where $E_e$ and $E_i$ are the excitatory and inhibitory reversal potentials, respectively, $g_e$ and $g_i$ are the excitatory and inhibitory conductances, and $g_{leak}$ is the leakage conductance. The values for $E_e$ and $E_i$ were set to 0.4 and -0.3, respectively, based on Borst *et al.* (1997). The conductances $g_e$ and $g_i$ were driven by the sum of the outputs of the rectified T5 units responding to the simulated tangential cell's preferred direction and the sum of the T5 units responding in the null direction, respectively (refer to 'G.C.' block in Figure 2.2). The value of the conductance $g_{leak}$ was empirically set to 3.5 S. We assumed a single-compartment cell model (see Section 3.3.2). The increase in the size of the input stimulus was simulated by scaling the output of 50 EMDs from an initial factor of 1 to a factor of 4 in equally spaced increments of 0.5. In a single-compartment model, this produces approximately the same results as increasing the pattern size by the same factors at sufficiently large values of spatial frequency.

Contrast sensitivity functions were computed as the inverse of the minimum contrast required for the simulated LPTC response to reach a particular percentage of the maximum amplitude response (criterion response) to sinusoidal stimulus. To convert the spatial frequency units of cycles/optic cartridge (derived from the model implementation) to units of cycles/degree, as reported in Dvorak *et al.* (1979), a conversion factor of 1.5 degrees/optic cartridge was used. This is in accordance with interommatidial angles for the fly *Lucilia sericata*, which vary from one to about two degrees depending on the region of the eye being examined (Land and Eckert, 1985).

## 3.3  Results

Most of the results on contrast saturation presented in this chapter were previously published in a short paper (Rivera-Alvidrez and Higgins, 2005).

### 3.3.1  Modeling Contrast Saturation

Measures of the responses of HS tangential cells to sinusoidal gratings which were initially stationary and then began moving suddenly are shown in Figure 3.1a (Egelhaaf and Borst, 1989). Both the steady-state response and the peak value of the transient response are plotted for two temporal frequencies (1 Hz and 10 Hz). The peak response amplitudes at both frequencies reach saturation faster than the steady-state responses. The peak responses for both frequencies seem to saturate at about the same contrast, while the steady-state response at the 1 Hz frequency saturates faster than the response at 10 Hz. Furthermore, the peak responses increase with higher temporal frequency, unlike the steady-state responses which are lower at higher frequencies.

In order to model contrast saturation, a saturating nonlinearity similar to the one used by Egelhaaf and Borst (1989) in an HR model was incorporated in the neuronally-based EMD model. Simulations with the nonlinearity inserted in different locations of the EMD model revealed that the results of the simulated LPTC predict the electrophysiological features of contrast saturation previously discussed only if the nonlinearities are placed in the locations indicated by the 'S' blocks in Figure 2.2. For instance, inserting the nonlinearities before the low-pass filters in the Tm9 pathways produced nearly equal peak response amplitudes for both simulated frequencies at all contrasts (data not shown).

Peak and steady-state responses of the simulated LPTC produced using the modified neuronally-based EMD model are shown in Figure 3.2a. The figure shows that the temporal frequency dependence of the peak and steady-state responses, as well as the crossing point between the two steady-state curves at a contrast of 0.5, are all predicted by the LPTC model. Sample responses of this model to sinusoidal stimuli at temporal frequencies of 1 and 10 Hz and a contrast of 0.25 are shown in Figure 3.2b.

Notice that while the temporal frequency dependence of the response measures is accurately modeled when the saturating nonlinearity is incorporated in the EMD model, the sigmoid does not explain the difference between the saturation levels reached by the peak and the steady-state
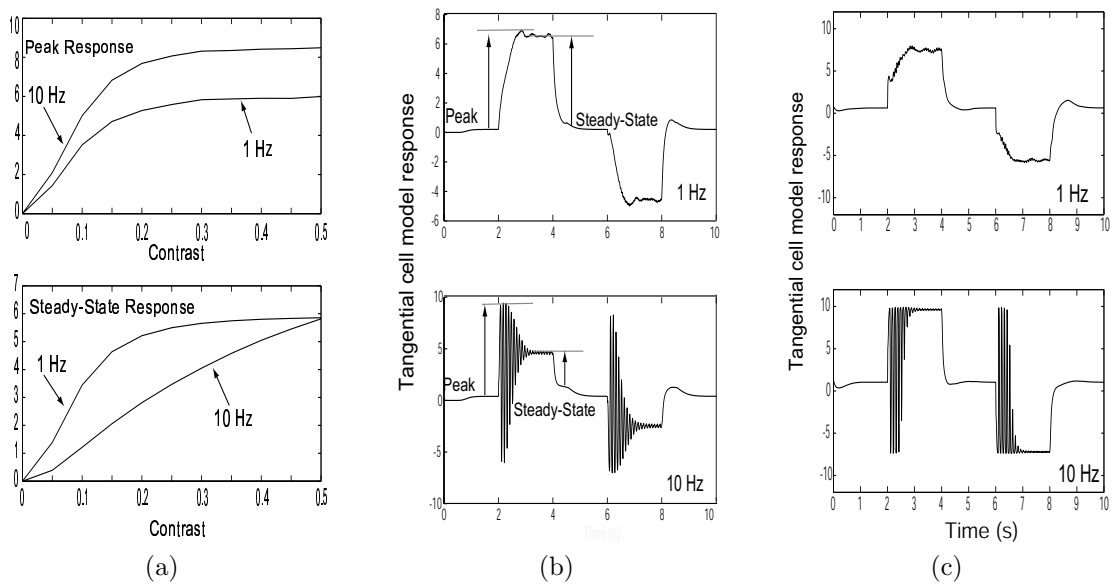
FIGURE 3.2. Contrast saturation in the simulated LPTC response. (a) Simulated LPTC response measures produced using the neuronally-based EMD model with saturation elements. The stimuli were sinusoidal gratings moving in the null direction at two temporal frequencies: 1 and 10 Hz. (b) Sample transient responses of the simulated LPTC to sinusoidal stimuli moving at 1 and 10 Hz with contrast of 0.25. For two seconds each, the stimulus was stationary, moved to the left, was stationary again and moved to the right. The peak and steady-state responses are marked in the plots. The steady-state value was computed as the mean response amplitude after the response had become stable. (c) Same stimulus as in **b**, except contrast is 0.95. Notice that the peak and the steady-state responses saturate to the same response level.
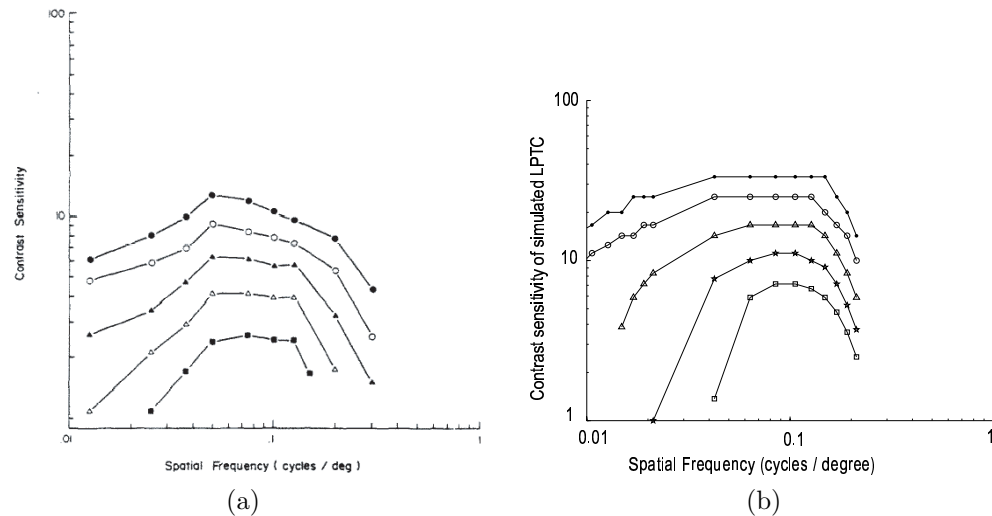
FIGURE 3.3. Contrast sensitivity functions for criterion response amplitudes (top to bottom lines) of 5%, 10%, 25%, 50% and 75% of maximum amplitude response for: (a) type IIa1 tangential cells, and (b) the simulated LPTC. The simulated LPTC response was computed using the neuronally-based EMD model incorporating saturating nonlinearities. Panel **a** reproduced without permission from Dvorak *et al.* (1979).

responses of the tangential cell. The sigmoid results in equal saturation levels for both the peak and the steady-state responses (consider peak and steady-state saturation levels at a frequency of 1 Hz in Figure 3.2a), unlike the electrophysiology which shows higher saturation levels for the peak response than for the steady-state response to the same stimulus (refer to 1 Hz saturation levels in Fig. 3.1a). Furthermore, the sigmoid is often found to distort the shape of the transients at high contrasts. This is illustrated in Figure 3.2c, which plots the response of the simulated LPTC for the two temporal frequencies at 95% contrast.

Contrast sensitivity functions were computed for the simulated LPTC response produced using the neuronally-based model with contrast saturation and compared to the functions obtained by Dvorak *et al* (1979) for type IIa1 tangential cells. Figures 3.3a and 3.3b show the CSFs from tangential cell recordings and from the simulated LPTC, respectively. The results from the LPTC model share several features with the electrophysiological data. The sensitivity of the model peaks at the same range of intermediate spatial frequencies as the CSFs of tangential cells, while showing similar degrees of attenuation at low and high frequencies. Like the electrophysiological data, the CSFs of the model show flat regions at intermediate frequencies. However, unlike the CSFs of tangential cells, the CSFs of the model do not become flatter as the criterion response amplitudes become larger (criterion response amplitudes increase from top to bottom in Fig. 3.3).

### 3.3.2 Modeling Saturation with Pattern Size

Saturation with pattern size was introduced into the computation of the simulated LPTC response by incorporating the biophysics of inhibitory and excitatory synaptic inputs, as discussed in Methods. As shown in Figure 3.4, the LPTC model accurately predicts a saturating response as the size of the stimulus is increased. Furthermore, the level of saturation reached by the simulated cell's mean response is a function of the stimulus temporal frequency. In agreement with the electrophysiology (refer to Fig. 3.1b), higher temporal frequencies result in lower saturation levels. Our implementation of pattern size saturation is based on a single-compartment cell model. This assumption has been
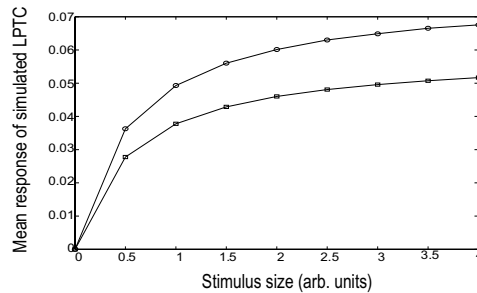
FIGURE 3.4. Mean response of the simulated LPTC to a sinusoidal pattern moving at two temporal frequencies: 35 Hz (circles) and 45 Hz (squares) as the size of the pattern is increased. The saturation level reached by the simulated LPTC response depends on the temporal frequency of the stimulus.

made by other authors (Borst *et al.*, 1995), and produces results qualitatively similar to those obtained if sixteen compartments (each one implementing Equation 3.2) are considered.

## 3.4 Discussion

A saturating nonlinearity was inserted into the neuronally-based model of elementary motion detection with parameters tuned to match electrophysiology from HS tangential cells (refer to Fig. 3.1a). The resulting LPTC model was found to produce results which looked very similar to the biological data, accurately predicting the shape and temporal frequency dependence of the tangential peak and steady-state responses to moving stimuli. Less success was achieved when modeling transient oscillations at high contrast levels (refer to Fig. 3.2c), which may suggest that while inserting a single saturating nonlinearity in pathways of the EMD model is a convenient simplification, it does not fully account for all the features of contrast saturation.

Contrast sensitivity functions (CSFs) of the LPTC model were computed and found to predict several features of the CSFs of tangential cells (refer to Fig. 3.3). While the sensitivity amplitudes, rates of attenuation at low and high frequencies and spatial frequency tuning of the neuronally-based CSFs were similar to the electrophysiology, the CSFs of the LPTC model do not become flatter at high contrasts (higher criterion response amplitudes). This feature of the electrophysiological data is likely due to a neuronal mechanism that holds sensitivity constant at high contrasts to compensate for attenuation that results from the optical filtering of the visual stimulus (Dvorak *et al.*, 1979). Evidence of such mechanism has been found in humans and is termed "contrast constancy" (Georgeson and Sullivan, 1975). This compensatory mechanism is not incorporated in the HR or the neuronally-based EMD models.

While Egelhaaf and Borst (1989) were able to produce similar results with the HR model, the results from the neuronally-based model have implications for the physiology of the insect. The simulations showed that there is only one location for the saturation element in the EMD model that produces results that match features of the electrophysiology from Egelhaaf and Borst (1989) at both transient and steady-state conditions. This implies that if the neuronally-based EMD model is correct in the relationships between the cells it incorporates, this saturation may arise in the synapses of the transmedullary cells (both Tm1 and Tm9) onto T5.

Saturation with increasing stimulus size was also successfully modeled with the incorporation of membrane potential biophysics into the computation of the simulated tangential cell response. This type of computation has been implemented in analog vision chips (Harrison and Koch, 1999), and has proven to be a powerful way to achieve this type of gain control with extremely low power consumption.

# Contrast Gain Adaptation

The topic of motion adaptation in tangential cell responses has been a subject of much research and debate in the last three decades. Motion adaptation results in a reduction of the magnitude of the LPTC response after exposure to moving stimuli (Maddess and Laughlin, 1985). Similar effects after motion adaptation have been reported in human psychophysics (Thompson, 1981; Clifford and Langley, 1996; Bex *et al.*, 1999), and in other mammals (Ibbotson *et al.*, 1998), suggesting the idea of common principles governing adaptation (Harris *et al.*, 2000). While it has been suggested that adaptation acts by reducing the contrast gain in the EMDs (Harris *et al.*, 2000), no neuronal mechanism has been proposed to explain how this change may take place or how it may relate to adaptation in mammalian vision systems.

In this chapter we identify a neuronal mechanism, namely frequency-dependent synaptic depression, which has been proposed to explain a number of adapting features in mammalian motion-sensitive neurons (Chance *et al.*, 1998), and use it to model motion adaptation. While synaptic depression has been studied mainly in spiking cells, we use the same principles to develop a simple model for depression in a graded synapse. By incorporating this synaptic model in a particular location in the neuronally-based EMD model, we show that we can predict with remarkable success the features of adaptation from various electrophysiological experiments.

## 4.1 Background and Previous Work

The response of the tangential cell H1 has been shown to be strongest at the onset of motion and to decay during continuous motion stimulation until a steady-state response level is reached. The rate of decay of the response was shown by Maddess *et al.* (1985) to be strongly dependent on the temporal frequency of the stimulus, and less sensitive to the contrast or to the spatial frequency of the grating. Importantly, this type of adaptation does not originate in the tangential cell itself, but it appears to be localized in the EMDs (Maddess and Laughlin, 1985).

Adaptation has also been studied by focusing on the effect that a high-contrast, high-frequency moving grating (also referred to as a "strongly adapting stimulus") has on a subsequent test stimulus, as shown in Figure 4.1. Three components of the adaptation induced by the high frequency stimulus were identified by Harris *et al.* (2000). Firstly, a rightward shift of the adapted contrast response curve with respect to the unadapted state was observed, which was referred to as a reduction in contrast gain. Secondly, a downward shift of the adapted curve was observed, referred to as an *afterpotential* or as the "waterfall effect" because of its similarity to the waterfall illusion in humans (Wolgemuth, 1911). The afterpotential is inhibitory if the cell was excited during the adapting period and excitatory if the cell was inhibited. The afterpotential appears to be activity dependent and directionally selective. Finally, a reduction in output range was observed, which produces a lower saturation level in the adapted curve, even when the afterpotential is subtracted. All three components appear to be generated through separate mechanisms, with contrast gain reduction contributing the most to motion adaptation (Harris *et al.*, 2000). Furthermore, while contrast gain reduction appears to be localized in the EMDs, the afterpotential and the output range reduction may originate in the tangential cell itself (Harris *et al.*, 2000). For this reason, we will focus on modeling contrast gain reduction using the neuronally-based EMD model.

Both Maddess *et al.* (1985) and Harris *et al.* (2000) reported that contrast gain reduction is more pronounced after adaptation with motion than with flicker. As shown in Figure 4.2, adaptation to
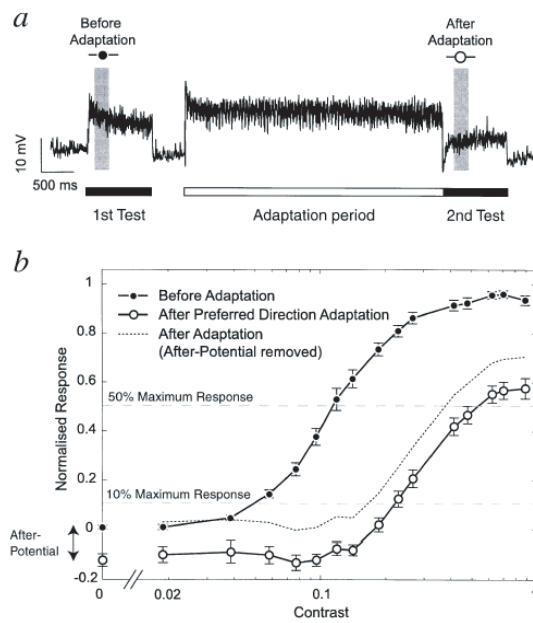
FIGURE 4.1. Motion adaptation in HS cells. (a) A sinusoidal test grating moving at 5 Hz (contrast = 30%) is presented before and after a strongly adapting stimulus (contrast = 95%, temporal frequency = 20 Hz). Both the test and the adapting stimuli move in the cell's preferred direction. The response to the test stimulus is significantly reduced after adaptation. (b) Normalized mean responses of HS cells to test stimulus before and after adaptation period, as the contrast of the adapting grating is varied. Responses are computed from the mean membrane potential 100 to 300 ms after the onset of the test stimulus. Reproduced without permission from Harris *et al.* (2000).
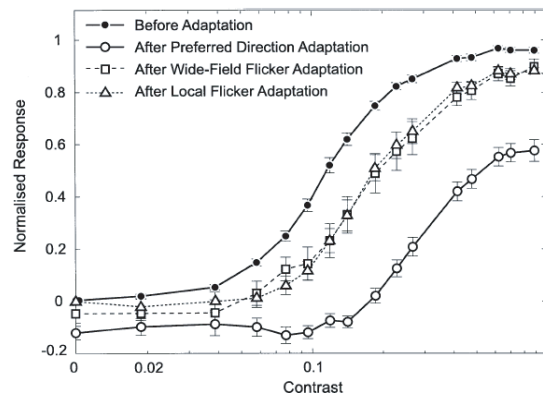
FIGURE 4.2. Adaptation with flicker versus motion. Normalized mean response of an HS cell to a test stimulus before adaptation (closed circles) and after adaptation with wide-field flicker (open squares), local flicker (open triangles), and preferred-direction motion (open circles). Adaptation with flicker is weaker than adaptation with motion. Reproduced without permission from Harris *et al.* (2000).

motion results in a more significant shift in the adapted curve than adaptation to both wide-field and local (counterphase) sinusoidal flicker. Moreover, Harris *et al.* (2000) also reported that contrast gain adaptation does not depend on the direction of motion. Figure 4.3 shows that when the afterpotential is accounted for, both adaptation with a stimulus moving in the preferred direction and adaptation with a stimulus moving in the anti-preferred direction result in similar reductions in contrast gain. Furthermore, the same contrast gain reduction is produced by a stimulus moving along the vertical axis, even though HS cells do not respond to vertical motion (Harris *et al.*, 2000).

Consider the contrast response of the unadapted cell in Figure 4.2. At high contrasts, the response of the cell becomes saturated, and variations in the stimulus contrast level result in little or no change in the response of the cell. At sufficiently low contrasts, the response of the cell is below the saturation threshold and variations in the contrast level produce large variations in the cell's response (the slope of the contrast response curve increases as the contrast is decreased). Saturation, therefore, reduces the cell's sensitivity to the stimulus contrast. A similar region of low sensitivity has been reported in the temporal frequency tuning of the cell at frequencies which elicit high response levels, and was also attributed to saturation (Harris *et al.*, 1999). Harris *et al.* (2000) proposed that the function of contrast gain reduction could be to "release" the motion pathway from saturation, allowing it to restore high sensitivity to fluctuations in the stimulus parameters. Harris *et al.* hypothesized that in order for contrast gain reduction to protect the system from saturation, it should occur before the EMD circuitry where this saturation arises. In Chapter 3, we introduced saturation elements in the inputs to the T5 cells of the neuronally-based EMD model to explain the saturating curves produced by the responses of LPTCs to increasing stimulus contrast. If the function of contrast gain reduction is to bring the system's response below the saturation threshold so that input sensitivity is restored, it would be reasonable to propose that it occurs before these saturation elements.

## 4.2   A Model of Contrast Gain Adaptation

Contrast gain reduction in fly visual interneurons reduces the cell's response during sustained motion stimulation. Such a response is similar to the type of responses exhibited in many mammalian cortical
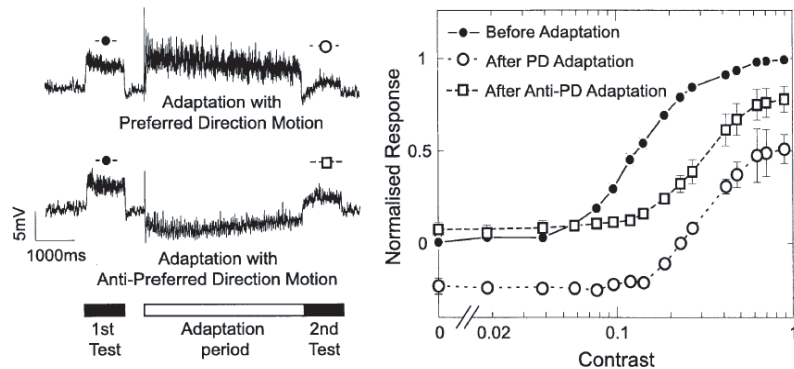
FIGURE 4.3. HS cell response to preferred-direction and anti-preferred direction adapting stimuli. Example traces are shown on left. On the right are shown normalized responses of HS cell to a test stimulus moving in the preferred direction presented before adaptation (closed circles) and after adaptation with a stimulus moving in the cell's preferred (open circles) and in the anti-preferred direction (open squares). Similar rates of adaptation are produced with preferred-direction and anti-preferred direction stimulation when the afterpotential is subtracted. Reproduced without permission from (Harris *et al.*, 2000).

neurons, including neurons in the primary visual cortex V1 (Chance *et al.*, 1998). These neurons respond to new high frequency stimuli in a stronger manner compared to their responses to sustained stimuli over the same frequency range. In rats, short-term synaptic depression (Abbott *et al.*, 1997; Varela *et al.*, 1997) has been identified in V1 neurons as being responsible for the reduction in their response to sustained stimuli (Chance *et al.*, 1998).

Given the parallels between the responses of the visual neurons in insects and mammals, it would be reasonable to postulate that a phenomenon such as synaptic depression could be occurring somewhere in the fly's EMD pathway. The first step to test this possibility would be to find a possible location in the neuronally-based EMD model where synaptic depression could be taking place. After considering the features of adaptation, the Tm1 transmedullary cell appears to be the most likely candidate. As discussed in Chapter 2, Tm1 is non-directional and responds to both vertical and horizontal motion, yet its inputs could allow it to differentiate motion from flicker. Adaptation could thus be taking place at the Tm1 synapses onto T5 and Tm9, before contrast saturation which has already been proposed in Chapter 3 to take place at the T5 inputs.

In V1, short-term synaptic depression has been modeled as a reduction in the magnitude of the postsynaptic conductance increase after a presynaptic action potential (Abbott *et al.*, 1997; Varela *et al.*, 1997; Chance *et al.*, 1998). In spiking cells, the rate of spikes is indicative of the strength of the response. The higher the rate of spikes, the stronger the depression becomes. In non-spiking cells, however, the strength of the response is encoded in the amplitude of the membrane voltage fluctuations with respect to the resting potential. Hence, it appears reasonable to model synaptic depression in Tm1 by making the reduction in the postsynaptic response proportional to the amplitude of the previous modulation that elicited the depression. If synaptic depression arises with each voltage modulation, then the rate of depression will be a strong function of the rate of modulations, which in Tm1 is equivalent to the temporal frequency of the moving stimulus. Because the amplitude of the modulations increases with contrast, the rate of depression will also be contrast dependent. In this model, high-contrast, high-frequency gratings will result in the strongest motion adaptation.

Our simple model for synaptic depression at the Tm1 synapses can be described as follows.

Depression is implemented as a gain factor with values in the interval [0,1], where a value of unity indicates no depression, and a value of zero indicates maximum depression. The depression gain factor multiplies the Tm1 activity to compute the postsynaptic response. Initially, the value of the depression gain factor is set to unity. During the time the cell response is rising and positive with respect to the resting potential, the gain factor decreases in value. While the cell response is decreasing or below the resting potential, the value of the depression gain factor is allowed to recover (towards unity). The postsynaptic effect of each cycle of activity in Tm1 is scaled down by the value of the gain factor at the beginning of the cycle. The decrease in the gain factor during rising responses is proportional to the amplitude of the rise.

Mathematically, let the Tm1 response (minus the resting potential) be $f(t)$. Let the time of the beginning of the rise of the last positive modulation in $f(t)$ be called $t_r$, and the time when this response stops rising and starts decaying be $t_d$ (see Figure 4.4). If $D(t)$ represents the depression gain factor, which is initialized to a value of unity, and $\tau_d$ the time constant of recovery, the model may be described as follows.

$$D(t) = \begin{cases} \frac{1}{\frac{1}{D(t_r)} + f(t) \cdot D(t_r)} & \text{if } ( \frac{\partial f(t)}{\partial t} > 0 \text{ and } f(t) > 0) \\ \frac{1}{1 + (\frac{1}{D(t_d)} - 1) \cdot e^{-\frac{(t - t_d)}{\tau_d}}} & \text{otherwise} \end{cases} \tag{4.1}$$

The postsynaptic response from Tm1 adjusted for depression ($Tm1_d$) would thus be:

$$Tm1_d = f(t) \cdot D(t_r) + V_{rest} \tag{4.2}$$

where $V_{rest}$ is the resting potential. Furthermore, if $f(t)$ is a sinusoid of frequency $f$ and amplitude $A$, then the magnitude of the scale factor $D(t_r)$ in each cycle $n$ of $f(t)$ can be described by the following nonlinear recursive equation:

$$D(t_r)_n = \frac{1}{1 + (A \cdot D(t_r)_{n-1} + \frac{1}{D(t_r)_{n-1}} - 1) \cdot e^{\frac{3}{4 f \tau d}}} \tag{4.3}$$

where $D(t_r) = 1$ during the first cycle ($n = 1$). Notice that because of the way we built the model, depression recovers during three quarters of every cycle (when $f(t)$ is decreasing or negative), hence the $\frac{3}{4}$ factor in the exponent in Equation 4.3. In order to maximize the depression elicited by $f(t)$, one needs to minimize $D(t_r)$, which can be accomplished by maximizing $A$ or by maximizing the frequency $f$. Decreasing $D(t_r)$ will, however, have the effect of decreasing the product $A \cdot D(t_r)$, which will decrease the maximum depression reached during the next cycle. Eventually, the reduction in the depression gain factor during a particular cycle will be fully recovered by the beginning of the next cycle, at which point $D(t)$ reaches a steady-state value. This eventual stabilization of synaptic depression in a steady-state level is illustrated in Figure 4.5 which shows the response of the Tm1 unit from the expanded neuronally-based EMD model (refer to Fig. 2.2), the postsynaptic response adjusted for depression $Tm1_d$, and the depression gain factor $D(t)$. Because in the neuronally-based EMD model all responses are with respect to a zero response level in the absence of stimulation (zero resting potential), subtraction of the resting response level is not necessary.

Note that this synaptic model is based on increasing depression only when the Tm1 response is rising above the resting potential. Because the model of Tm1 is symmetric in its response to positive and negative modulations with respect to a resting potential, the same results would have been produced if we had used the negative modulations to compute depression. Another possibility would be to increase depression whenever the response of the cell is increasing, regardless of whether the response is positive or negative with respect to the resting potential. Because of the symmetry in Tm1, this would only result in doubling $A$ in equation 4.3 and in reducing the time of recovery
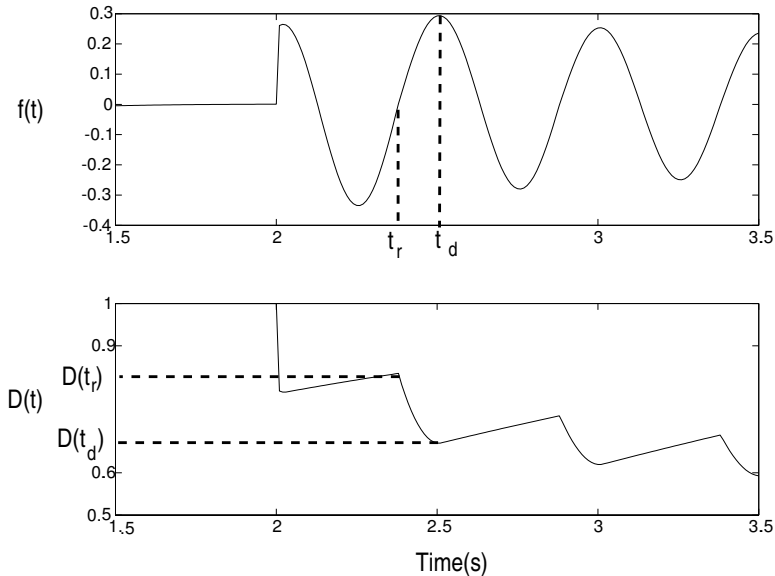
FIGURE 4.4. A model of depression in Tm1 synapses. The top plot shows the response of $f(t)$ (Tm1 minus resting potential) after stimulation with a sinusoidal grating moving at 2 Hz (contrast $= 0.5$). The time of the beginning of the rise of a positive modulation $t_r$ and the time the response begins to decay $t_d$ are indicated for one cycle. The bottom plot shows the depression gain factor $D(t)$ for the same stimulus. The levels of depression at the times $t_r$ and $t_d$ are marked on the plot.

to one half of a cycle. Reducing the time constant of recovery and using a scaled version of $A$ would thus generate the same results as the model proposed.

In order to compare our model for contrast gain reduction with LPTC electrophysiology, we present the results of a simulated tangential cell which was produced using the neuronally-based EMD model incorporating frequency-dependent synaptic depression in the Tm1 synapses.

## 4.3   Methods

In every experiment we used the expanded neuronally-based model including contrast and pattern size saturation (see Chapter 3). Two different values for the slope of the sigmoid were used depending on the stimulus protocol. All experiments which included the presentation of a mean luminance stimulus were produced using a sigmoid function with parameters provided in Section 3.2. In order to reduce the effect of the sigmoid on the response oscillations produced when the pattern is shown stationary before motion stimulation, the slope of the sigmoid $C_3$ was reduced from 43 to 20 to produce the results shown in Fig. 4.9b. Adaptation was implemented as described in Section 4.2. The time constant of recovery $\tau_d$ was set to 1.2 sec. The adapting algorithm was implemented in the Tm1 synapses onto T5 and Tm9, as shown in the blocks labeled 'A' in Figure 2.2.

## 4.4   Results

Figure 4.6a shows the H1 response to a square-wave grating which moved at constant speed for 4 seconds at different contrast levels after being adapted to a mean luminance stimulus. The response of the simulated cell is shown in Figure 4.6b. Similar adaptation rates are produced by the real cell and the model, especially at the two extreme frequencies: 2 Hz and 16.7 Hz. Notice that the
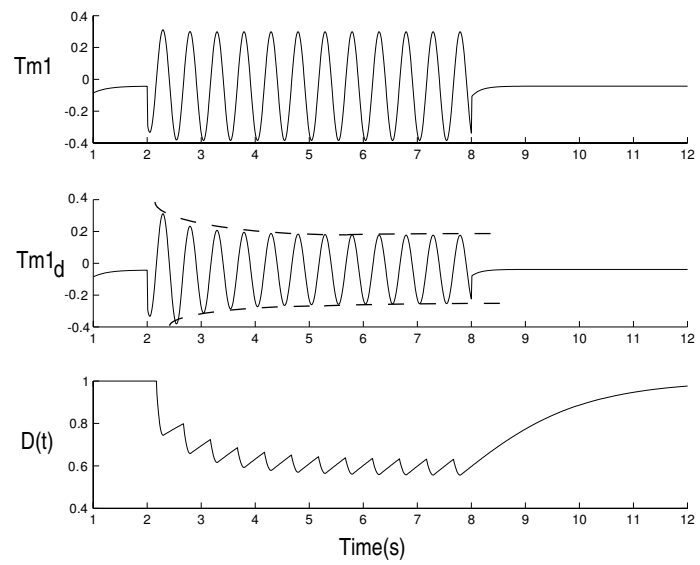
FIGURE 4.5. Synaptic depression in Tm1. Plots show the unaltered Tm1 response (top), the Tm1 response adjusted for depression $Tm1_d$ (center), and the corresponding depression gain factor $D(t)$ (bottom). The stimulus was a sinusoidal grating moving at a temporal frequency of 2 Hz (contrast = 0.5). The dotted traces in the $Tm1_d$ plot emphasize the envelope produced by the effect of the depression gain factor on the Tm1 response. Notice the eventual stabilization of depression in a steady-state level.

responses produced are both a function of the Tm1 depression rates and of contrast saturation. Contrast saturation tends to reduce the effect of adaptation at frequencies that elicit high response levels, as shown in the 2 Hz plots. Importantly, the effect of adaptation appears more pronounced for high contrast, high frequency stimuli, as expected. Furthermore, as the frequency and the contrast are increased, the depression reaches a steady-state level faster, a feature more clearly shown in Figure 4.7 which plots the time-course of the depression gain factor $D(t)$ for the same stimuli.

The responses of H1 and of the model to motion stimuli moving in the null direction are shown in Figures 4.8a and 4.8b, respectively. Because H1 exhibits a low spontaneous firing rate, which is further reduced during motion stimulation in the null direction, Reisenman *et al.* (2003) presented a stimulus moving in the preferred direction in a separate visual area within the cell's receptive field when producing the results shown in Figure 4.8a. This had the effect of increasing the dynamic range of the cell's response to motion in the null direction by increasing the resting firing rate (Reisenman *et al.*, 2003). Notice that the rates of adaptation produced by the model are a very close match to the electrophysiology at contrasts of 19% and 95%. At the lowest contrast of 11%, the firing rate of H1 is not significantly different from the adjusted resting rate. At this contrast level the model response shows depolarizations at the beginning and the end of the motion stimuli. These depolarizations have been previously reported in tangential cell recordings of HS cells (see below), although Egelhaaf and Borst (1989) noted that they were not consistently produced in all preparations.

Figure 4.9 shows intracellular recordings of an HS cell, which was stimulated with a sinusoidal grating moving in the null direction after the grating was shown stationary. To the right of the recordings are model responses to the same stimulus protocol. In order to avoid distorting the response oscillations by the sigmoid used to model contrast saturation, the slope of the sigmoid was reduced to produce this plot (see Methods). Notice that the oscillations produced in the model are larger than the oscillations in the electrophysiology. They are however similar in size and duration to the oscillations produced by versions of the HR model with similar filter time constants (Harris and O'Carroll, 2002). Like the electrophysiology, the model response also shows depolarizations at the onset of motion which were not predicted by the HR models (Harris and O'Carroll, 2002). The presence and size of these depolarizations was found to depend on the initial phase of the grating. Averaging the results of five experiments with random initial phase, as was done to produce the plots, had the effect of reducing the amplitude of the depolarizations when compared to some of the ones observed at particular phase values. Figure 4.9c shows the response of the model to the same type of stimuli, except that a mean luminance stimulus was presented before motion stimulation to avoid oscillations which obscure the cell's mean response. Notice the similar time-course in the model response and the electrophysiology, especially at the highest frequencies. Depolarizations before and after motion stimulation are similarly produced.

Adaptation in the model is directionally insensitive, as expected from the properties of Tm1. Figures 4.10a and 4.10b show the simulated LPTC response to a test stimulus before and after a period of strong adaptation with a high-frequency, high-contrast grating moving in the preferred direction (4.10a) and in the anti-preferred or null direction (4.10b). Notice that the response to the second test stimulus is attenuated by the depression elicited by the adapting grating, similar to the tangential cell recordings (refer to Fig. 4.1). Moreover, decreasing the frequency of the stimulus from 20 Hz during the adapting phase to 5 Hz during the second test phase increases the time that the depression has to recover during subsequent cycles. As a result, the Tm1 depression gain factor $D(t)$ recuperates to a higher value during the test stimulus (see bottom plots in Fig. 4.10), which causes the response of the simulated LPTC to increase during the test phase. This increase is also seen in LPTC recordings (refer to Fig. 4.1).

Finally, we test adaptation with motion versus flicker. Figure 4.11a plots the steady-state response of the model during the test stimulus before and after adaptation with local flicker (counterphase) and with motion, as the contrast is increased. While adaptation with flicker appears weaker for all the contrasts tested, the difference between motion and flicker is not as pronounced as in

(a)



(b)

FIGURE 4.6. Adaptation during continuous preferred-direction motion stimulation. (a) H1 recordings during motion stimulation with a square-wave grating moving at three different temporal frequencies and three contrast levels in the cell's preferred direction. A mean luminance stimulus was shown between presentations of moving stimuli. (b) Simulated tangential cell response to the same stimulus protocol. The model incorporates depression in the Tm1 synapses onto T5 and Tm9. Panel **a** reproduced without permission from Reisenman *et al.* (2003).
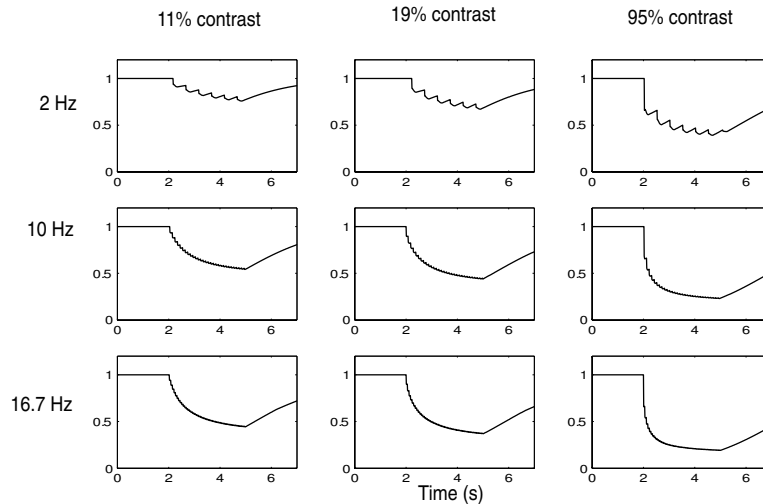
FIGURE 4.7. Depression gain factor $D(t)$ for the stimulus protocol of Figure 4.6. Increasing either the contrast or the temporal frequency of the visual stimulus reduces the values reached by $D(t)$ and the time needed for it to stabilize at a steady-state level.

the electrophysiology (refer to Fig. 4.2). If instead of the two-dimensional EMD model we use the one-dimensional model (refer to Fig. 2.2), the response of Tm1 to motion is further emphasized from flicker. This is shown in Figure 4.11b, which shows a more significant difference between adaptation with motion and flicker (see Discussion).

## 4.5 Discussion

A model for visual motion adaptation based on synaptic depression in mammalian vision cells was incorporated in the Tm1 synapses of the neuronally-based EMD model. Even though the aim was to produce the most simple model that could enable us to compare the rough features of the simulation results with the electrophysiology, the results obtained match closely, in many cases, the time course followed by the cell's response. Our model explains the strong temporal frequency dependence of adaptation, the eventual stabilization of adaptation to a steady-state level, and the observed recovery of LPTC responses from a strongly adapted state induced by a high-frequency high-contrast grating (refer to Figure 4.10). In addition, as discussed below, new observations arising from the work provide insight and possible explanations about complex features of adaptation, which have not been previously addressed.

*Contrast saturation reduces the contrast dependence of the rates of adaptation in LPTC responses to sustained motion stimulation.* While Maddess *et al.* (1985) reported a weak dependence of H1 adaptation rates during continued motion stimulation on contrast, high-contrast high-frequency gratings are found to induce strong adaptation based on the effect they have on a subsequent test stimulus (Harris *et al.*, 2000). Our results show that even though adaptation is highly dependent on contrast, as shown in Figure 4.7, this dependence is obscured in the simulated cell responses by contrast saturation, which tends to reduce the effect of adaptation as the contrast is increased. Thus, while in some cases the responses to a moving grating at different contrast levels appear to simply be scaled versions of each other (refer to 10 Hz plots in Figures 4.6a and 4.6b, for example), the levels and rates of adaptation may be significantly affected by contrast (refer to Figure 4.7). Because adaptation in the model occurs before contrast saturation, this contrast dependency, though
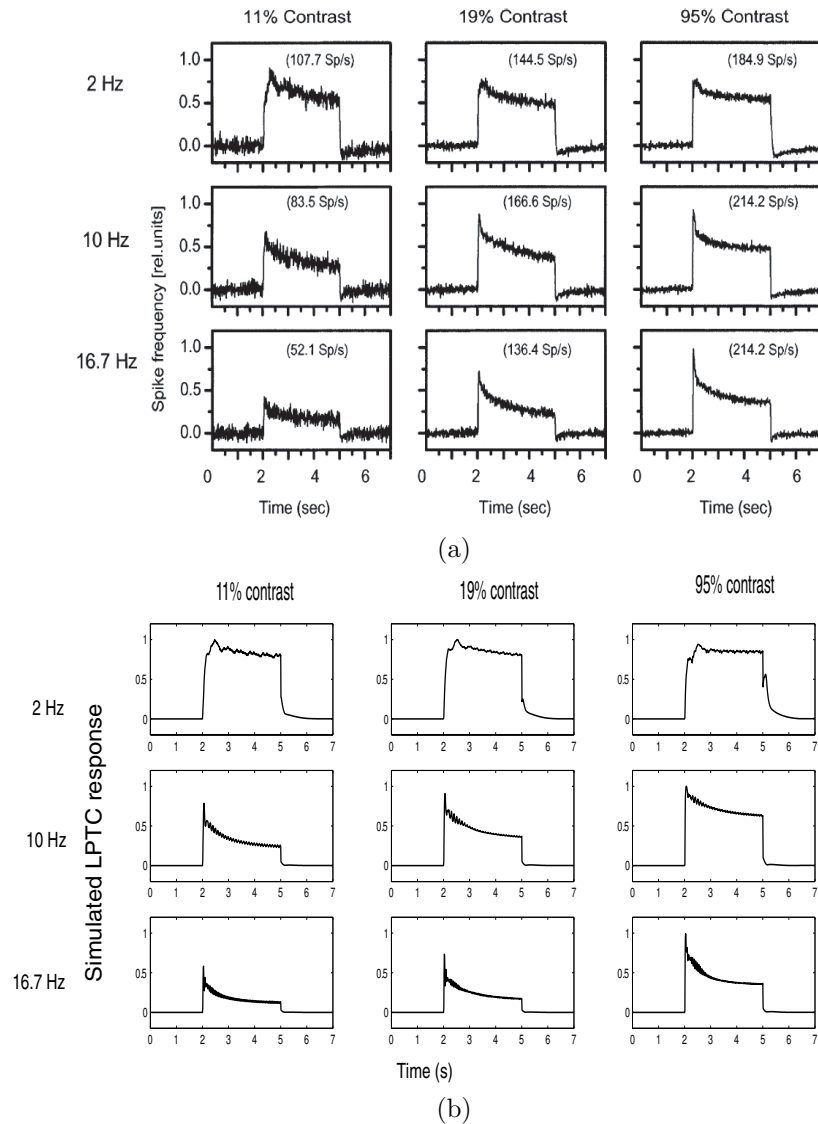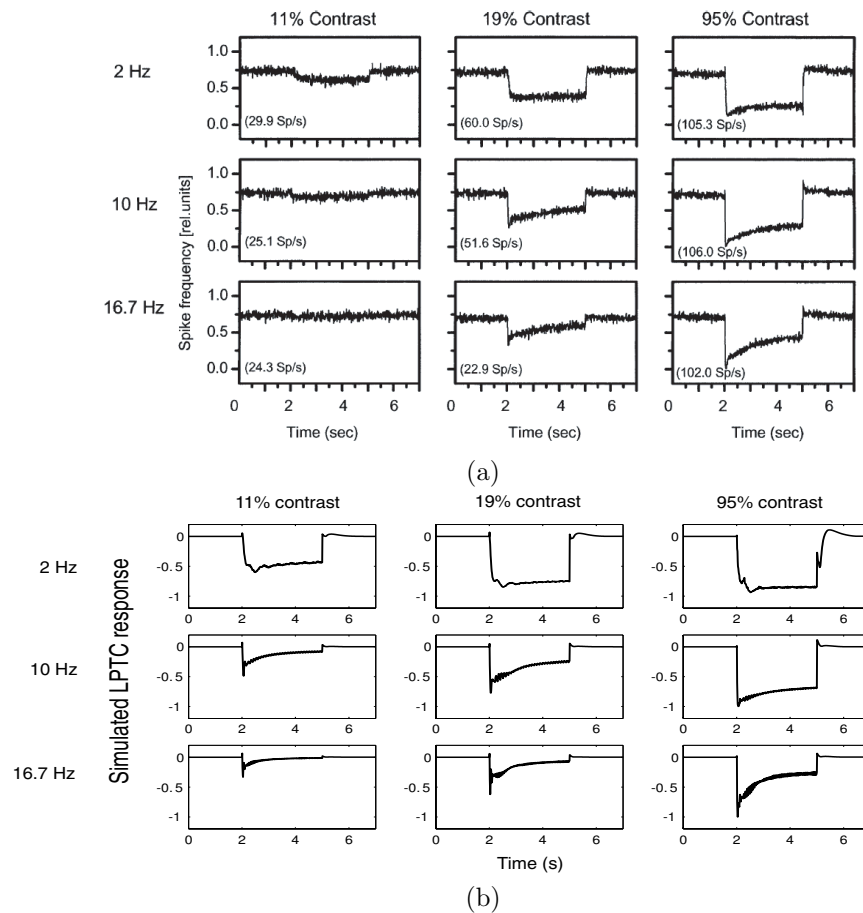
Figure 4.8. Adaptation during continuous null-direction motion stimulation. (a) H1 recordings during motion stimulation with a square-wave grating moving at three different temporal frequencies and three visual contrasts in the cell's null direction. The stimulus was blanked to a mean luminance level between presentations of moving stimuli. (b) Simulated tangential cell response to the same stimulus protocol. The model incorporates depression in the Tm1 synapses onto T5 and Tm9. Panel **a** reproduced without permission from Reisenman *et al.* (2003).
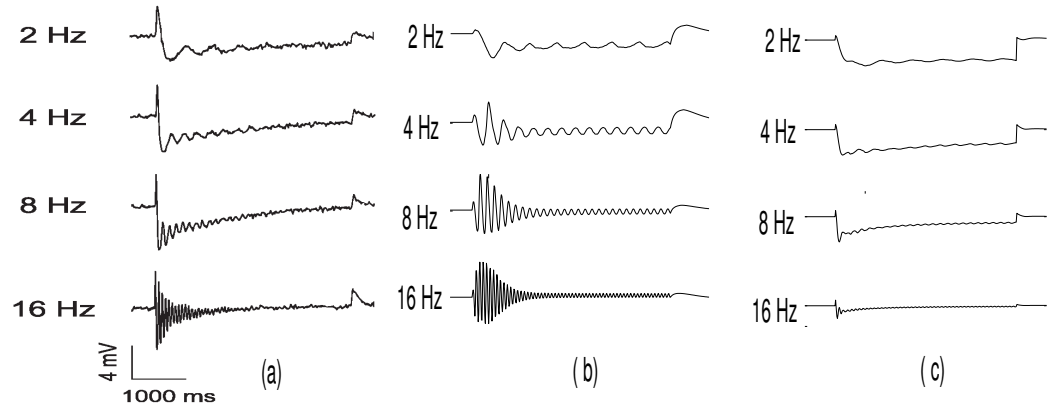
FIGURE 4.9. Comparison of responses from an HS cell and from the LPTC model to null-direction motion stimulation. Intracellular recordings of an HS cell (a) and LPTC model responses (b and c) to sinusoidal gratings moving in the cell's null direction at various temporal frequencies (contrast = 10%). In panels **a** and **b** the grating was shown stationary before motion stimulation producing response oscillations (see Methods). In panel **c** a mean luminance stimulus was presented. Panel **a** reproduced without permission from Egelhaaf and Borst (1989).
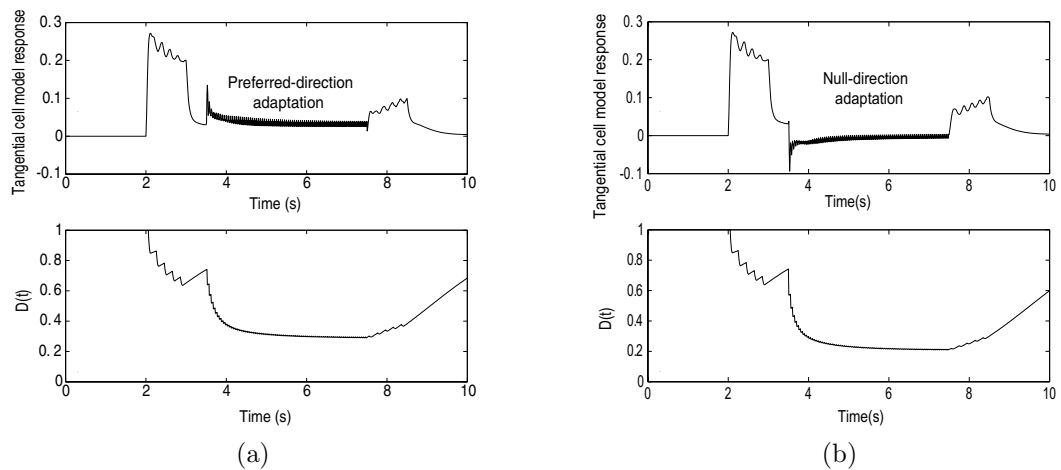


FIGURE 4.10. LPTC model response to a test grating (30% contrast, 5 Hz temporal frequency) before and after strong motion adaptation with a sinusoidal grating (95% contrast, 20 Hz temporal frequency), which is moving in the preferred direction (a) and in the anti-preferred or null direction (b). Top plots show the simulated tangential cell response. Bottom plots show the time-course of the depression gain factor $D(t)$. Compare to HS cell recordings in Figure 4.1 and 4.3.
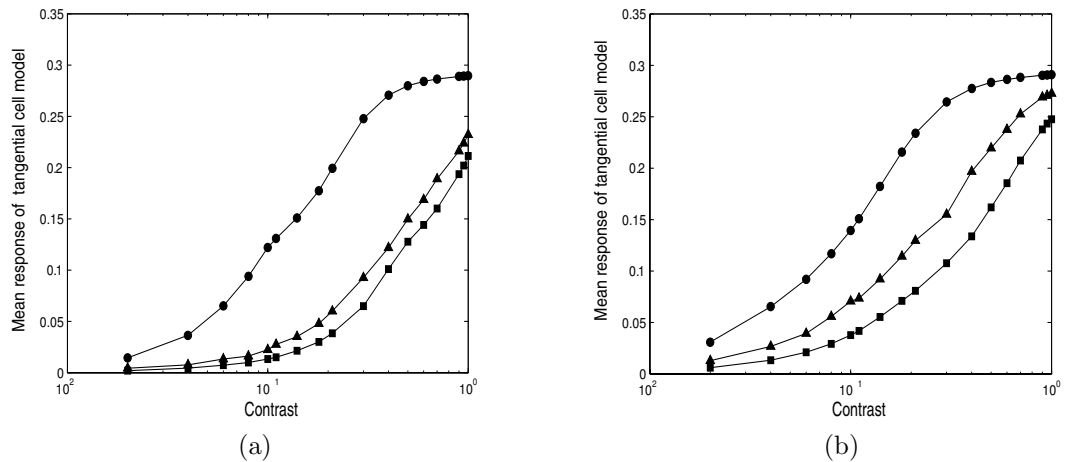
FIGURE 4.11. Adaptation with flicker versus motion. (a) Mean response of the simulated tangential cell before adaptation (circles) and after adaptation with local flicker (triangles) or with motion (squares). As in Harris *et al.* (2000), the response was computed as the mean value 100 ms to 300 ms after the onset of the test stimulus. (b) Same as panel **a**, except that the one-dimensional EMD model was used (see Chapter 2). Compare to Figure 4.2.

not evident in the cell's response, will be reflected in the magnitude of the reduction of the cell's response to a low-contrast test grating.

*Adaptation with flicker versus motion.* Adaptation with sinusoidal counterphase flicker was found to be weaker than adaptation with motion, but this difference was not as pronounced as in the electrophysiology. A more comparable difference was produced if instead of the two-dimensional EMD model, we used the one-dimensional model where T1 is computed by adding amacrine signals from only two neighboring photoreceptors (refer to Fig. 2.2), as opposed to the complete hexagonal array. Doing so reduces the rates of adaptation produced with flicker stimuli by reducing the response of T1 to flicker. It may be possible to produce similar results with the two-dimensional model after better developing the early visual processing model stages. In particular, it is likely that amacrine cells interact with one another, and it is conceivable that such interactions result in an emphasis of motion versus flicker through some type of inhibition. Such idea may also result in a stronger Tm1 response to motion than to wide-field sinusoidal flicker. In the current Tm1 model, little if any difference is produced between these two types of stimuli (data not shown). More biological data is required to find out whether the Tm1 response to wide-field (sinusoidally modulated) flicker is weaker than its response to motion.

*The origin of synaptic depression.* Synaptic depression may arise through postsynaptic or presynaptic conditions. Postsynaptic conditions may involve receptor desensitization (Takahashi *et al.*, 1995), while presynaptic depression may arise from reduced efficacy of the release machinery or from depletion of releasable vesicles (Neher, 1998). Because the properties of the Tm1 synapses or similar synapses in this part of the fly's visual ganglia are largely unknown, we cannot distinguish between these possibilities. The large size and abundance of vesicle pools observed in the Tm1 synapses, however, make vesicle depletion an unlikely source of depression in Tm1 (Strausfeld, personal communication, 2005).

*Parallels between insect and mammalian motion detection.* Similarities between adaptation in fly interneurons and adaptation in mammalian neurons and human psychophysics have been previously

noted (Harris *et al.*, 2000). Our work suggests that the mechanism of adaptation through short-term synaptic depression may be common to insect tangential cells and to visual motion-sensitive neurons in the primary visual cortex of rats. How these two species could have arrived to the same neural principles may be explained in terms of evolutionary convergence, where unrelated species under similar environmental constraints independently arrive through evolution to the same computational solutions. Evolutionary convergence in neural sensory systems is widespread (for a review see Nishikawa, 2002).

# Adaptation in the EMD filters

In addition to contrast gain reduction, motion adaptation has also been proposed to result in dynamic changes in the EMD filter parameters (de Ruyter van Steveninck *et al.*, 1986; Borst and Egelhaaf, 1987). Specifically, the time constant of the filters has been said to become shorter after the presentation of a high-frequency moving stimulus. This idea, however, has been challenged by a number of findings (Harris *et al.*, 1999), including modeling work which suggests a different explanation for results previously explained in terms of a reduction in the filter time constant (Harris and O'Carroll, 2002). In 2003, Borst *et al.* presented modeling data and new electrophysiology results (Reisenman *et al.*, 2003) supporting the idea of changes in the filter time constant as an explanation for the shortening of transient responses measured both in the response of the cell to very brief image motion, and in the cell's response to sustained motion stimuli. In this chapter, we show that most of the data in Reisenman *et al.* (2003) can be predicted by the expanded neuronally-based model without incorporating any dynamic changes in the filter parameters. Moreover, we show that the arguments used to refute similar modeling work do not apply to our model.

## 5.1 Background and Previous work

Most of the evidence in support of changes in the time constant of the EMD filters originates from "impulse response" experiments. The stimulus protocol used to produce these results typically involves abruptly stepping the visual stimulus in the LPTC preferred direction, or alternatively, stimulating the cell with very brief image motion. Tangential cells respond to that type of stimulus with a transient depolarization which decays exponentially (see Figure 5.1a). In 1986, de Ruyter van Steveninck *et al.* showed that if the image step is preceded by motion stimulation during an adapting phase lasting several seconds, the rate of decay of the transient is strongly dependent on the speed of the adapting grating. As shown in Figure 5.1a, the duration of the transient becomes shorter when the speed of the adapting stimulus is increased. If the canonical HR model shown in Fig. 1.6a is used to model EMDs, the time constant of decay of the simulated cell's impulse response is equal to the time constant of the first-order low-pass filter in the model regardless of previous stimuli. This fact was interpreted as evidence suggesting that the shortening of the transient was produced by a shortening of the filter time constant after motion adaptation (de Ruyter van Steveninck *et al.*, 1986). According to the canonical HR model, a shortening of the EMD filter time constant would translate into a shift of the EMD frequency optimum towards higher temporal frequencies.

While the idea of dynamic adaptation of filter parameters was supported in many publications (de Ruyter van Steveninck *et al.*, 1986; Borst and Egelhaaf, 1987; Egelhaaf and Borst, 1989; Clifford *et al.*, 1997; Reisenman *et al.*, 2003; Borst *et al.*, 2003), in 1999 Harris *et al.* presented substantial evidence against it. In particular, Harris *et al.* showed that the temporal frequency tuning of a moving test stimulus remained roughly the same regardless of whether the test stimulus was presented before or after adaptation with a high-frequency moving grating (see Figure 5.1b). In 2002, Harris and O'Carroll presented modeling results produced with an HR model with high-pass filters in all its inputs (refer to Fig. 1.6b), which they referred to as the "high-pass" model. Their simulations incorporated an "imbalanced subtraction" (unequal weights were assigned to the two outputs of the multipliers in Figure 1.6b) to produced the simulated LPTC response. The impulse response produced using the high-pass model (see Figure 5.2) predicted changes in the rate of decay
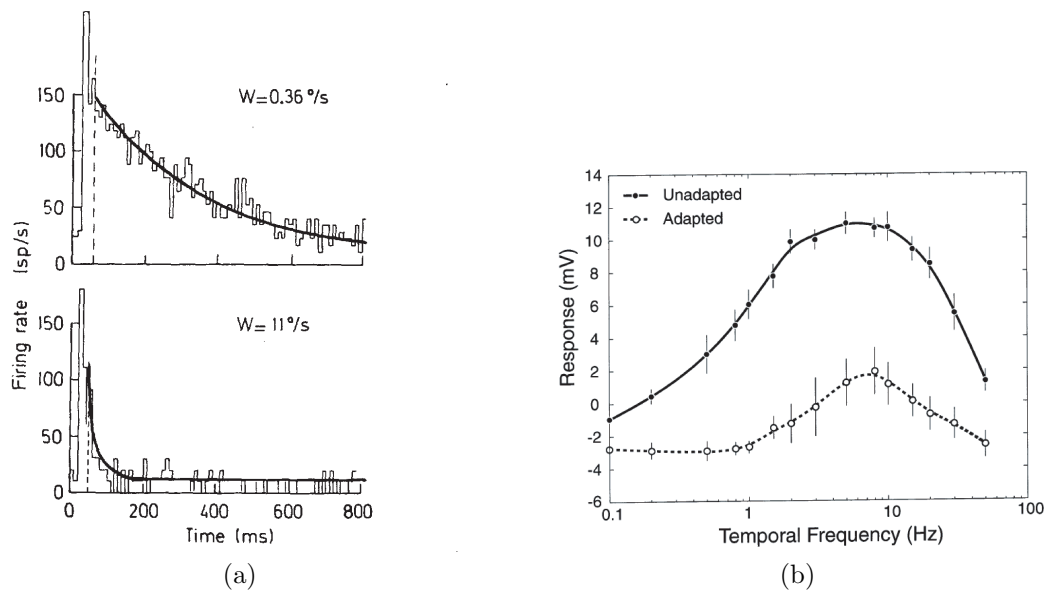
FIGURE 5.1. The effect of motion adaptation on LPTC impulse responses and frequency tuning. (a) Average H1 impulse responses. The stimulus was a square-wave grating (contrast = 40%) which moved with velocities of 0.36 deg/sec (top) and 11 deg/sec (bottom), remained stationary for 200 ms and was abruptly stepped 6 degrees in the cell's preferred direction. The duration of the transients is reduced after high speed motion adaptation. (b) Temporal frequency tuning of HS cell before motion adaptation (solid line) and after motion adaptation (broken line). Responses were computed from the average response 100 ms to 250 ms after the onset of a test grating presented before and after a strongly adapting stimulus. The frequency tuning remains roughly the same before and after motion adaptation. Panels **a** and **b** reproduced without permission from de Ruyter van Steveninck *et al.* (1986) and Harris *et al.* (1999), respectively.
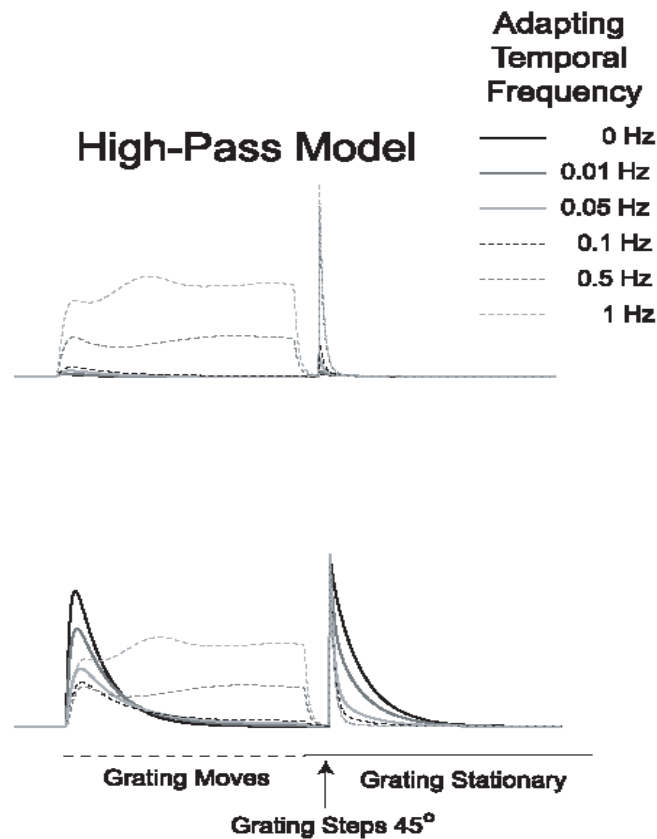
FIGURE 5.2. The impulse response of the high-pass model. The stimulus was a sinusoidal grating which moved during 1.8 seconds at various temporal frequencies, and was stationary during a period of 200 ms, after which its phase was stepped 45 degrees in the preferred direction. Unnormalized responses are shown in top plot. Bottom plot shows responses normalized to match peak amplitude during image step. The transients decay faster as the frequency of the moving grating is increased. Reproduced without permission from Harris and O'Carroll (2002).

of the LPTC impulse response similar to those reported by de Ruyter van Steveninck *et al.* (1986) without any type of change in the time constant of its filters.

The results obtained with the high-pass model were explained in terms of the afterimage effect (Harris and O'Carroll, 2002). Afterimages, first described by Maddess *et al.* (1986), refer to the profound changes in the response of tangential cells to subsequent motion stimuli after the presentation of slowly moving or stationary adapting gratings. The presentation of a stationary grating, as shown in Figure 5.3, produces strong transient oscillations in the LPTC response to a moving test stimulus with decay time constants as long as 900 ms. These transient oscillations are not present when a mean luminance stimulus precedes the stimulation with motion. The afterimage oscillations last longer when the adapting grating is stationary or moving slowly and are reduced as the speed of the grating is increased (Harris and O'Carroll, 2002). Based on the afterimage effect, it follows that the presentation of an image step after stimulation with a high frequency moving grating would result in a short impulse response, while abruptly stepping the image after it was shown stationary for a number of seconds would result in a longer transient (Harris and O'Carroll, 2002). The afterimage
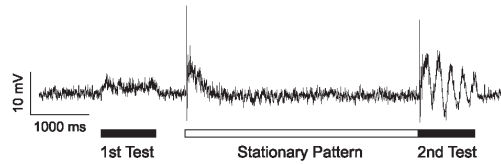
FIGURE 5.3. Illustration of the afterimage effect. The first moving test stimulus (5% contrast, 5 Hz) was shown after blanking the visual stimulus to mean luminance, while the second test stimulus was shown after a stationary grating (65% contrast) was presented for several minutes. The presentation of a stationary grating produces strong transient oscillations in the LPTC response to the second test stimulus. Reproduced without permission from Harris and O'Carroll (2002).

effect is therefore consistent with the impulse response data.

Borst *et al.* (2003), who support the idea of changes in the time constant of the EMD filters (Borst and Egelhaaf, 1987; Egelhaaf and Borst, 1989), refuted the data obtained with the high-pass model with the following two arguments. Firstly, the impulse response of an HR model with high-pass filtered inputs can be mathematically shown to be zero if the grating was shown stationary for a sufficiently long period of time (to allow filters to reach their steady-state) before the image step. This is in contrast to LPTC electrophysiology, which shows a strong impulse response regardless of the duration of the stationary phase of the stimulus. While the high-pass model does produce an impulse response when the stationary pattern is shown for a brief period (refer to Fig. 5.2), Borst *et al.* (2003) pointed out that the shortening of the transients only became evident after normalization, before which the amplitude of the transients were minuscule. Secondly, the response of the high pass model to a moving sinusoidal grating is the same before and after spatial integration by the simulated tangential cell. This contradicts calcium imaging (Single and Borst, 1998) and small aperture experiments (Egelhaaf *et al.*, 1989) that show that local modulations appear in the tangential cell inputs and only disappear after spatial integration. According to Borst *et al.* (2003), these two arguments suggest that the EMD input pathways are not all high-pass filtered, and so the high-pass model should not be used to explain the impulse response data.

Reisenman *et al.* (2003) showed that the response of tangential cells to the sudden onset of sustained motion stimulation (referred to as the "step response") produces transients which decay at faster rates as the contrast of the stimulus is increased. These transients have superimposed oscillations due to the afterimage effect when the grating is shown stationary before the stimulation with motion (see Figure 5.4a), but not when a mean luminance stimulus was presented before the moving grating (see Figure 5.4b). In both cases, the transient components were said to decay faster as both the contrast and the temporal frequency of the stimuli were increased. The fact that this reduction in the duration of the transients was observed to occur even when the oscillations produced by the afterimage effect were not present (Fig. 5.4b) was used as an argument to refute the involvement of the afterimage effect in the shortening of the transients. The reduction in the duration of the transient components was explained in terms of changes in the time constant of the EMD filters.

Reisenman *et al.* (2003) argued that these transients followed time courses similar to the impulse response transients at low and high contrasts. This argument was supported by the presentation of impulse response data, which showed that increasing the stimulus contrast resulted in a more pronounced reduction in the duration of the transients (refer to Figure 5.5). Borst *et al.* (2003) proposed a different version of the HR model with low-pass filters in two of its pathways and high-pass filters in the other two (refer to Fig. 1.6c), which through adaptation of the high-pass filter time constant could explain the impulse and step response transient reduction without significantly

changing the cell's frequency tuning.

In this chapter, we present simulation results using the neuronally-based EMD model which show that most of the data in Reisenman *et al.* (2003) can be produced by the simulated LPTC without incorporating changes in the EMD filter parameters.

## 5.2    Methods

All simulations were run using the expanded neuronally-based EMD model incorporating pattern size saturation with parameters provided in Section 2.3. Neither contrast saturation nor contrast gain reduction was modeled when producing the impulse response data. Using a sigmoid to model contrast saturation was found to distort the shape of the transients. Contrast gain reduction was disabled (by setting the depression gain factor $D(t) = 1$ at all times) in order to be able to evaluate the impulse responses without the effects of adaptation. Disabling adaptation allowed us to compare the impulse response of our model with LPTC impulse responses (in Fig. 5.5) which were manipulated in order to subtract the effects of adaptation (Reisenman *et al.*, 2003). The impulse responses shown were produced after averaging the results of 50 experiments with random initial phase. Both contrast saturation and contrast gain reduction were modeled when simulating step responses (in Fig. 5.8), as described in Chapter 4.

## 5.3    Results

### 5.3.1    Impulse Response Data

To produce the impulse response of the model we used a stimulus protocol similar to the one used by Reisenman *et al.* (2003) to generate the responses in Figure 5.5. A square-wave grating moved for three seconds at various temporal frequencies, was stationary for 200 msec, and moved at 10 Hz for 20 msec. Figure 5.6 shows the unnormalized responses for stimuli at two contrast levels. The pathways in the neuronally-based EMD model allowing a sustained component of the photoreceptor signal (the "relaxed high-pass filters", Figure 2.2) allow the simulated tangential cell to have an impulse response amplitude comparable to the amplitude of its response to motion stimulation. While the impulse response of our simulated LPTC is in some cases smaller than its step response, the impulse responses produced by our model are definitely much larger than the unnormalized impulse responses of the high-pass model (refer to Fig. 5.2).

The contrast dependence of the rate of decay of the simulated LPTC impulse response is illustrated in Figure 5.7, which shows that increasing the contrast of the adapting stimulus results in a more significant difference between the unadapted and the adapted impulse response. This is the same dependence found in the H1 recordings (refer to Figure 5.5), but not in the simulations with the high-pass model (Harris and O'Carroll, 2002). As expected, increasing the frequency of the adapting grating produces shorter impulse responses. Our simulations show that in order to produce any significant difference between the impulse response of the adapted and the unadapted tangential cell model, there needs to be an imbalanced subtraction of the tangential cell EMD inputs with opposite preferred directions. This is true both for our model and for the high-pass model. In our model such imbalanced subtraction is already incorporated in the computation of the simulated LPTC response due to the unequal excitatory and inhibitory reversal potentials which multiply the rectified T5 outputs with opposite preferred directions in Equation 3.2.

### 5.3.2    Step Response Data

Reisenman *et al.* (2003) reported that transient components in the H1 step responses decay faster when the contrast is increased. While our model does not clearly predict any reduction in the transient oscillations of the step response when the pattern is shown stationary before motion stimulation as in Fig. 5.4 (data not shown), any transient components in the step responses without oscillations

**(a)**



**(b)**
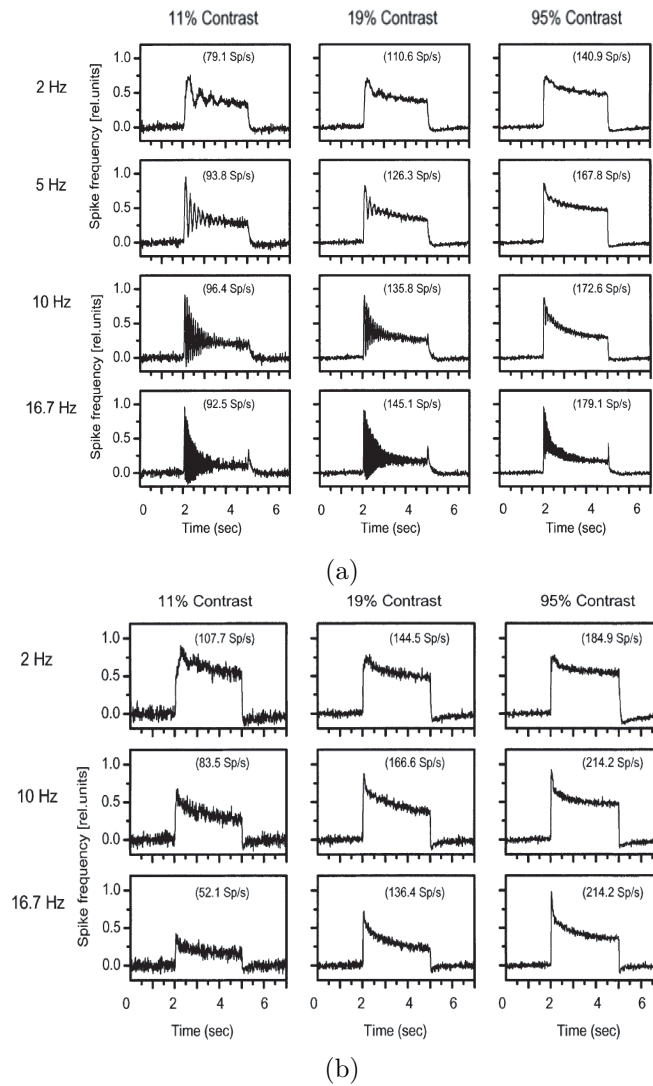
FIGURE 5.4. Adaptation in the step responses of H1. (a) H1 recordings during motion stimulation with a square-wave grating moving at various temporal frequencies and three visual contrasts in the cell's preferred direction. The stimulus was shown stationary between phases of sustained motion stimulation. Notice a reduction in the transient oscillations of the responses as the contrast and frequency of the stimulus are increased. (b) Same as panel **b** except that the stimulus was blanked to a mean luminance level between presentations of motion stimulation. Notice the responses reach steady-state faster at high contrasts and high temporal frequencies. Reproduced without permission from Reisenman *et al.* (2003).
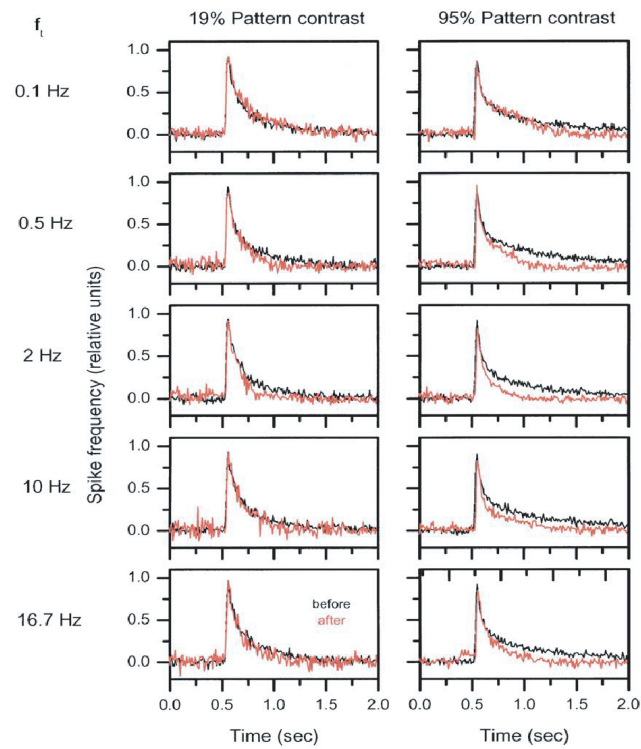
FIGURE 5.5. Impulse responses of H1 before adaptation (black traces) and after adaptation (gray traces) with moving gratings at various temporal frequencies and at two different contrast levels. Responses are normalized to their maximum. Notice that a more pronounced difference between the adapted and the unadapted traces is present when the contrast is increased. Reproduced without permission from (Reisenman *et al.*, 2003).
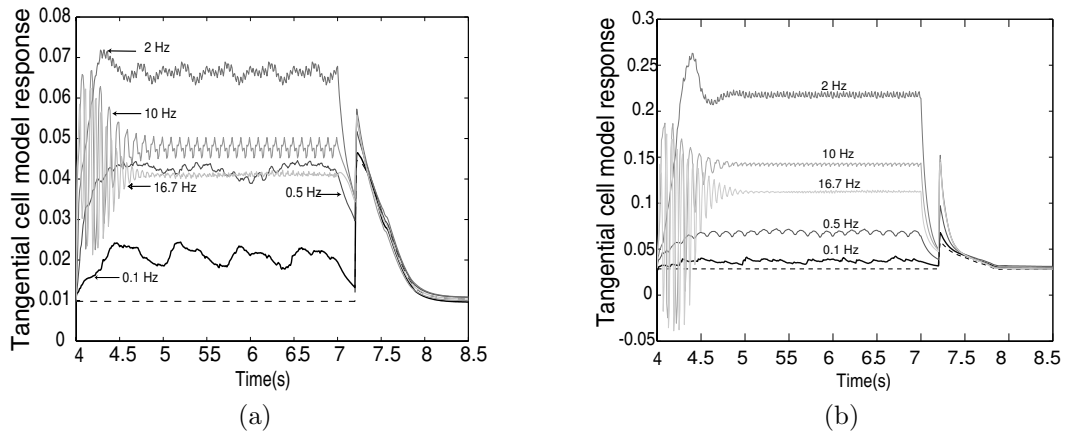
FIGURE 5.6. Unnormalized impulse responses of the simulated tangential cell after motion adaptation. A square-wave grating moved for three seconds at various temporal frequencies, was stationary for 200 msec, and moved at 10 Hz for 20 msec. The plots show superimposed unnormalized responses for a contrast of 18% (a) and 95% (b). The adapting grating moved at temporal frequencies of 0 Hz (broken line), 0.1 Hz, 0.5 Hz, 2 Hz, 10 Hz, and 16.7 Hz. While no significant difference in the impulse responses at low contrast can be appreciated, a reduction in the duration of the transients with increasing frequency can be seen at high contrast.

(i.e. a mean luminance stimulus was presented between phases of motion stimulation) appear to be at least partially explained by our model incorporating contrast gain reduction. Figure 5.8 (reproduced from Figure 4.6), shows that the transient components of the step responses of the simulated LPTC decay faster when the contrast and the frequency of the stimulus are increased (compare 2 Hz plot with 11% contrast to 16.7 Hz plot with 95% contrast). This reduction in the duration of the transient decay is due to our model of contrast gain reduction which predicts that increasing the contrast and frequency of the grating results in rates of depression that reach a steady-state levels faster.

## 5.4  Discussion

We presented simulation results with the expanded neuronally-based EMD model showing that the reduction in the duration of the impulse response transients can be adequately explained without implementing dynamic changes in the time constant of the EMD filters. Furthermore, the expanded neuronally-based model does not have any of the drawbacks cited to refute the results obtained with the high-pass model. Relaxed high-pass filtering (with a low-pass component) enables the model to produce robust impulse responses. The response of the neuronally-based model, unlike the high-pass model, does exhibit local modulations which are reduced through spatial integration in the simulated tangential cell.

Our results show the same contrast dependence of the impulse response as the electrophysiology. Note that this dependency cannot be explained in terms of the afterimage effect, as the duration of afterimage transients increases with increasing contrast levels (Harris and O'Carroll, 2002). While it is unclear how this dependency arises, through our simulations it was found that imbalanced subtraction is required both for our model and for the high-pass model to generate impulse responses decaying at different rates depending on the frequency of the adapting grating. Perhaps the most important lesson from our work is that in a highly nonlinear system, the results from impulse
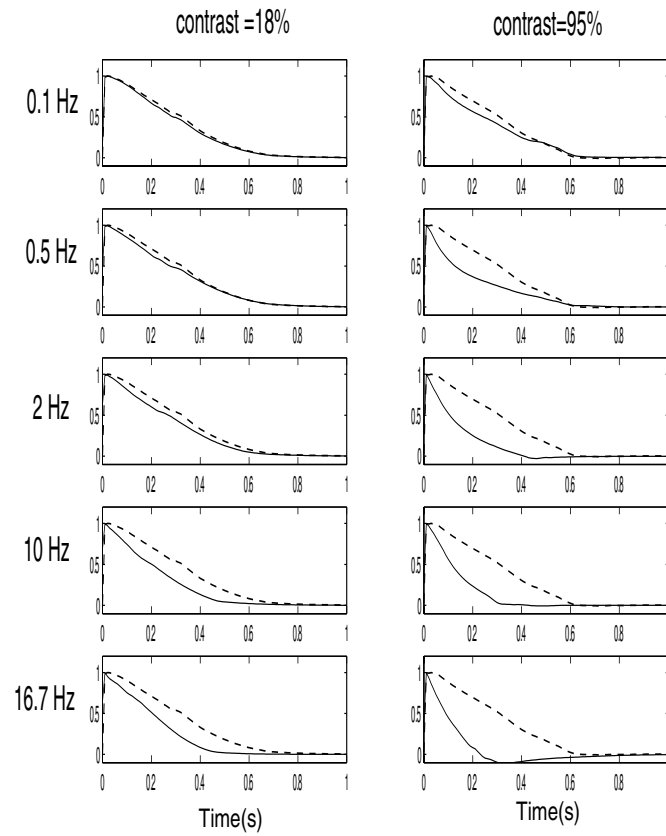
FIGURE 5.7. Normalized impulse responses from Figure 5.6 produced at contrasts of 18% and 95% (compare to Figure 5.5). The broken line shows the unadapted response (temporal frequency of adapting grating was set to zero). The responses were normalized to their maximum and the sustained component of the response was subtracted. Increasing the contrast of the grating results in a more significant difference between the adapted and the unadapted impulse response.
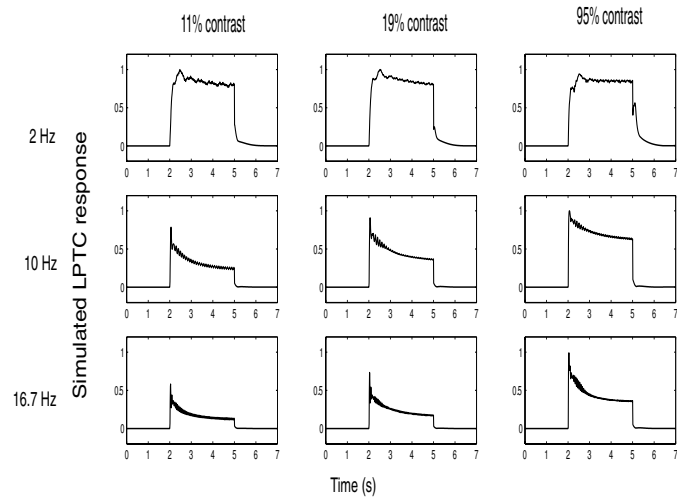
FIGURE 5.8. Step responses of the simulated LPTC with an EMD model incorporating contrast gain adaptation. A mean luminance stimulus was presented before motion stimulation with a square-wave grating at various contrast levels and temporal frequencies. The model incorporates depression in the Tm1 synapses onto T5 and Tm9 (see Chapter 4). Compare to Figure 5.4b.

response experiments may be affected not only by the time constant of the filters but also by a number of other factors.

Reisenman *et al.* (2003) also reported a reduction in the afterimage oscillations present in the tangential cell step response as the contrast is increased, and propose that such reduction is produced by a shortening of the time constant of the EMD filters. While we are unable to model the transient oscillations produced by the afterimage effect at high contrasts, we showed that the expanded neuronally-based model which incorporates contrast gain adaptation accounts for any transient components of the H1 response in experimental paradigms that do not produce oscillations.

Our simulations show that changes in time constant of the EMD filters are not necessary to explain a number of results attributed to them. Explaining the reduction in the afterimage oscillations at high contrasts may require a deeper understanding of the early visual processing stages where this oscillations appear to originate and a more elaborate model of contrast saturation.

# Redundancies in the Fly Visual Motion Pathways

While the foundations of the neuronally-based EMD model are supported by available histological, anatomical, and electrophysiological results, not all of the data is conclusive and some degree of speculation was involved into the development of the model. The desire to obtain more conclusive physiological information about the motion detection pathway is challenged by the small size and inaccessibility of many of the cells possibly involved. Recently, genetic tools which can block specific cell types by the selective expression of neural toxins have been used to block cells believed to be involved in motion detection. The idea is that if the cell being blocked is in the motion detection pathway, then the flies with the genetic removal will suffer from impairment of behaviors which require the ability to detect motion, such as the optomotor response. Behavioral experiments with flies in which two cells proposed to be involved in motion detection (the lamina monopolar cell L2 and the basket T-cell T1) were genetically removed produced somewhat unexpected results.

In this chapter we show the results of simulations with the expanded neuronally-based EMD model which may explain the outcome of recent genetic experiments. Our results provide additional evidence in support of the model while revealing redundancies in the input pathways that may result in a remarkably robust motion detection system.

## 6.1 Background and Previous Work

The involvement of the lamina monopolar cell L2 in motion detection has been a subject of debate. L2 is postsynaptic to the achromatic photoreceptors R1 through R6 in the retina (for a review see Strausfeld and Nässel, 1980) and both its apparent connectivity to transmedullary cells (Strausfeld, 1970) and functional imaging studies with dexoglucose (Bausenwein and Fischbach, 1992; Buchner and Buchner, 1984) suggest an important role for L2 in motion detection. In 1989, however, Coombe *et al.* reported a poor correlation between the degeneration of the lamina monopolar cells L1 and L2 and optomotor responses in the fly mutant *Vam, vacuolar medulla.* Because this mutant also suffers severe degeneration in the outer medulla (Coombe and Heisenberg, 1986), which could also affect the optomotor response, the results from these experiments were not conclusive.

Keller (2002) presented results from behavioral experiments with flies in which L2 had been genetically blocked by the selective expression of tetanus neurotoxin (TNT), a toxin that impairs evoked neurotransmitter release. Keller conducted a number of behavioral experiments aimed at quantifying the optomotor response in flies expressing a TNT line exclusively in L2 (TNT-flies) and in control specimens. In one type of experiment, flies immobilized such that they could only move their heads were shown a moving visual stimulus to elicit an optomotor response in the form of a head rotation. The steady-state angle reached by the head was reported as a measure of the strength of the response. No statistically significant difference was found between the TNT-flies and the controls. In a second type of experiment, flies which could walk on a styrofoam ball (refer to Figure 1.5b) were shown the same type of moving stimuli, while the rotations of the ball were carefully measured. The amount of rotation was then reported as a measure of the magnitude of the walking optomotor response. The results of this experiment are shown in Figure 6.1. A clear and statistically significant reduction in the magnitude of the response was found between the TNT-flies and the control specimens, at a wide range of temporal frequencies.
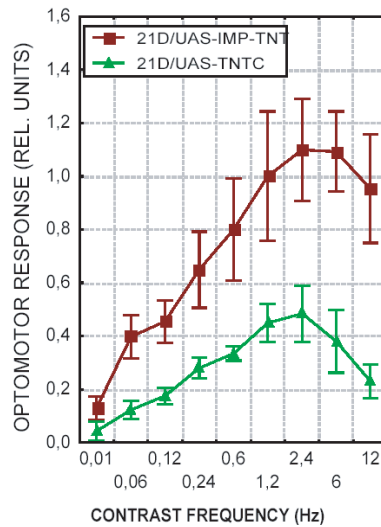
FIGURE 6.1. Optomotor responses in walking for flies with blocked L2 (21D/UAS-TNTC in legend, TNT-flies in text) and controls (21D/UAS-IMP-TNT in legend). A statistically significant reduction in the optomotor response was found at all temporal frequencies tested. Reproduced without permission from Keller (2002).

Because the TNT-flies were still able to detect motion after the L2 removal, Keller (2002) concluded that L2 is not necessary for motion detection, but that, given the reduction in the measure of the walking optomotor response, it may still be involved in the computation. Similarly, preliminary experiments (Heisenberg, unpublished data, 2005) suggest that motion detection is not fully impaired in flies in which the basket T-cell T1 is genetically blocked, and the results of the behavioral experiments involving these flies may be very similar to those obtained with the L2 removal.

In this chapter we show that the expanded neuronally-based EMD model (refer to Fig. 2.2) produces results that agree with the behavioral results from genetically-altered flies by presenting the responses of a simulated LPTC computed either with the original EMD model, or with EMD models lacking L2 or T1. LPTC responses are highly correlated with the optomotor behavioral response, and are believed to be largely responsible for this behavior.

## 6.2    Methods

Simulations were run with the two-dimensional version of the expanded neuronally-based EMD model incorporating contrast and pattern size saturation (see Chapter 3 for details), and contrast gain adaptation as described in Chapter 4. When specified, either the L2 or the T1 units in Figure 2.2 were deleted from the model. Deleting L2 resulted in T1 being the only input to Tm1. Similarly, deleting the T1 unit resulted in L2 being the only Tm1 input.

## 6.3    Results

The responses of a simulated LPTC before and after removing the cell L2 from the expanded neuronally-based EMD model are shown in Figure 6.2. While removing L2 reduced the magnitude of the simulated LPTC response, the removal does not impair its directional selectivity. This result is due to the fact that in the absence of L2, motion information is still transmitted to Tm1 from the T1 unit. Figure 6.3 shows that the effect of the L2 removal on the steady-state response of

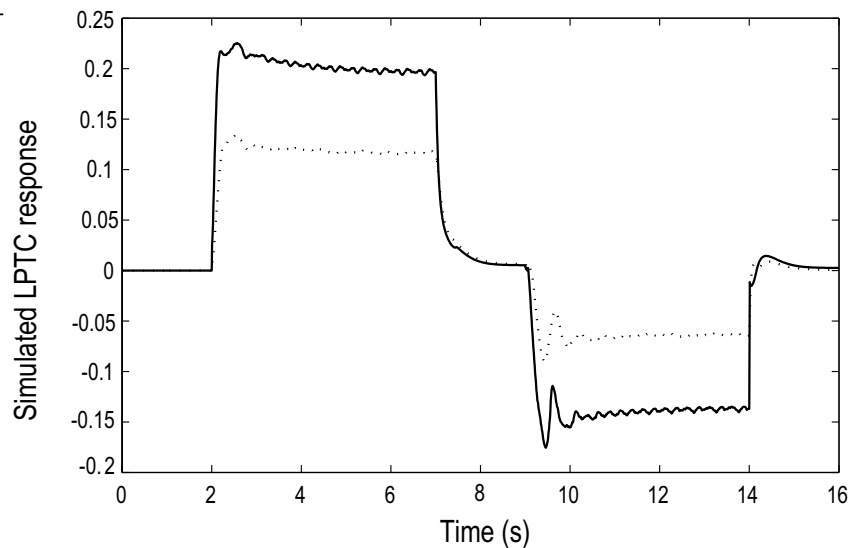FIGURE 6.2. Responses of the simulated tangential cell computed with L2 (solid line) and without (dotted line) to a sinusoidal stimulus moving in the horizontal direction at a temporal frequency of 2 Hz (contrast = 20%). The stimulus moved in the preferred direction for five seconds, was stationary for two seconds, and moved in the null direction for five seconds. A mean luminance stimulus was presented during the first and last two seconds of stimulation. Removing L2 reduced the magnitude of the LPTC response.

the model LPTC depends on the contrast and temporal frequency of the visual grating. Contrast saturation makes the EMD outputs less sensitive to changes in the signal level at high contrasts. Moreover, the L2 deletion results in a shift of the simulated LPTC temporal frequency optimum towards lower frequencies. Because L2 is high-pass filtered (refer to Figure 2.2), its contribution to the model response is higher at high temporal frequencies, and the response reduction after L2 is removed is therefore more significant as the frequency of the stimulus is increased.

Removing T1 from the input pathways of the neuronally-based model produced similar results, although a smaller reduction in the amplitude of the simulated LPTC response was predicted. Figure 6.4 shows the steady-state responses of the original EMD model, and of a model lacking T1. Notice that a shift of the simulated cell's frequency optimum towards higher temporal frequencies is predicted after the T1 removal. This shift arises from the fact that in the model all T1 inputs are low-pass filtered, which means that the contribution of T1 to the overall response is more significant at low temporal frequencies. As in the results with the L2 removal, increasing the contrast of the visual stimulus decreased the effect of removing T1.

Figure 6.5 plots the steady-state responses of the complete model, a model lacking L2, and a model lacking T1, as the spatial frequency of the visual grating is varied. While removing L2 from the model did not change the spatial frequency tuning of the simulated cell, removing T1 from the model results in a shift of the cell's spatial frequency optimum towards higher frequencies. This result can be explained by the fact that in the complete model or in a model lacking L2, the Tm1 output is computed as a sum a spatial pool of photoreceptors (refer to Fig. 2.2), reducing the high-frequency content of the individual input signals. Removing the T1 input from Tm1, results in Tm1 receiving only the signal from a single photoreceptor (transmitted by L2), allowing high-frequency information to be used in the computation of motion.
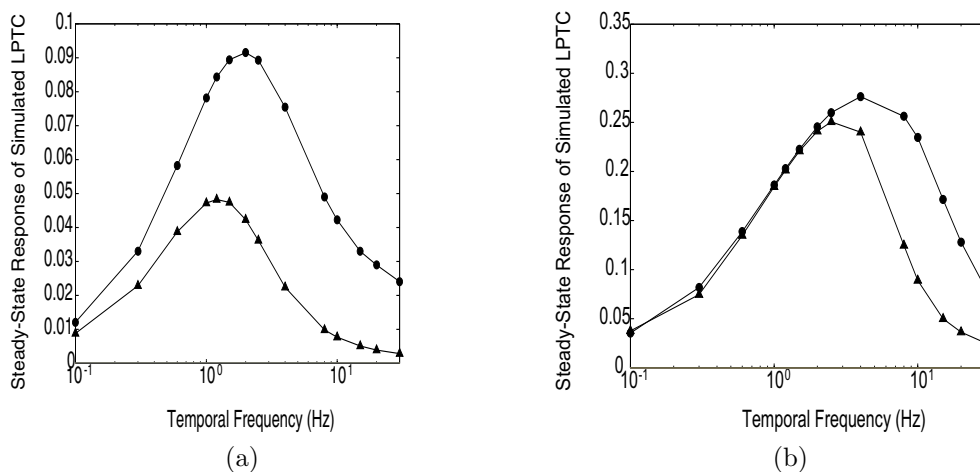
FIGURE 6.3. Steady-state responses of the simulated LPTC computed with L2 (circles) and without (triangles) to sinusoidal stimuli moving at various temporal frequencies and at contrast levels of 5% (a) and 95% (b). The steady-state value was computed as the mean response amplitude during the last second of five seconds of motion stimulation in the preferred direction. Notice that the reduction in the LPTC response after the L2 deletion is greater at low contrasts and high temporal frequencies.
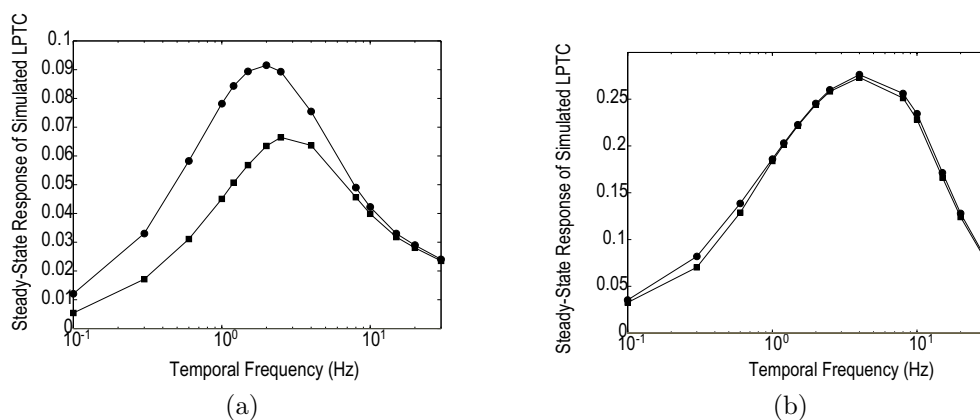


FIGURE 6.4. Steady-state responses of the simulated LPTC computed with T1 (circles) and without (squares) to sinusoidal stimuli moving at various temporal frequencies and at contrast levels of 5% (a) and 95% (b). The steady-state value was computed as the mean response amplitude during the last second of five seconds of motion stimulation in the preferred direction. The reduction in the LPTC response after the L2 deletion is greater at low contrasts and low temporal frequencies.
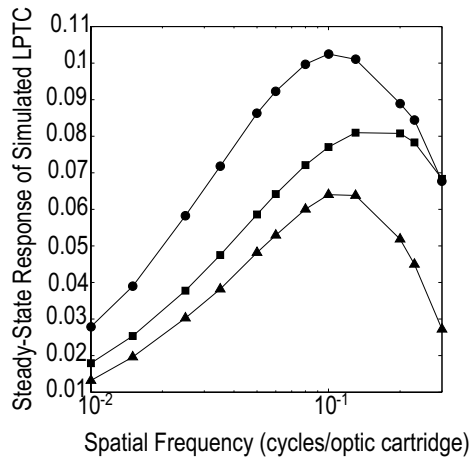
FIGURE 6.5. Steady-state responses of the complete model (circles), the model without L2 (triangles) and the model without T1 (squares), as the spatial frequency of the grating is varied. The temporal frequency of the stimulus was 1 Hz and the contrast was 10%. Removing T1 from the model results in a shift of the simulated LPTC spatial frequency optimum towards higher frequencies.

## 6.4  Discussion

The results of simulations with the expanded neuronally-based EMD model are consistent with the results of behavioral experiments with genetically-altered flies. Both the results of the behavioral experiments and our simulations suggest a reduction in the magnitude of the tangential cell response to motion after the deletion of either T1 or L2. Our simulations show that the simulated tangential cell response does not lose its directional selectivity if either of these cells is removed from the model. In addition, the magnitude of the reduction in the tangential cell response after the removal is a function of the stimulus temporal and spatial frequencies and of the stimulus contrast. This could explain why in some behavioral experiments no significant difference was found between the TNT-flies and the control specimens.

In addition to a reduction in the LPTC response to motion, our results predict other effects of removing T1 from the motion detection pathway that may be used to guide future experiments. The simulations show that the T1 removal results in a shift of both the temporal and the spatial frequency tuning of the simulated LPTC towards higher frequencies. Furthermore, because T1 provides the model with the only DC or sustained component of the response, removing T1 would significantly decrease the magnitude of the tangential cell impulse response (see Chapter 5). Importantly, because contrast saturation obscures the changes in the Tm1 signal level after the T1 or the L2 deletion, our results show that the changes in the properties of the LPTC response described are more evident when the contrast of the visual stimulus is low.

Although having both T1 and L2 in the motion-detection pathway does not seem to be crucial for the ability of tangential cells to detect directional motion or for the optomotor response, both cells are necessary in our model for the transmedullary cell Tm1 to compute non-directional motion by comparing signals from neighboring photoreceptors in T1 to the local signal from L2 (Higgins *et al.*, 2004). Non-directional motion from Tm1 may underlie insect behavioral use of image speed (see Chapter 7), and we have proposed a possible role for Tm1 in contrast gain adaptation (see Chapter 4). Moreover, because T1 adds the signals from a spatial pool of photoreceptors, having T1 in the motion detection pathway may both increase the detector's response to motion at lower spatial frequencies, and increase the signal-to-noise ratio by sampling the signals from several photoreceptors. Since

noise is one of the most important considerations of early visual processing (for review, see Burton, 2000), such a system would ensure that a reliable signal is provided to the detector even in low luminance conditions when the high frequency information from L2 may not be as reliable.

The resulting system is also robust in that, as was shown in the experiments, it can still operate when one of the input pathways is removed. This remarkable robustness may be an evolutionary advantage, protecting the fly's ability to detect motion and the behaviors that depend on it against genetic defects or synaptic malfunctions.

# A MECHANISM FOR SPEED ESTIMATION

A number of behavioral experiments suggest the idea that insects may use the apparent angular image speed on their eyes for various tasks, including navigation (Srinivasan *et al.*, 1996) and landing (Srinivasan *et al.*, 2000). However, the responses of most cells involved in motion detection depend both on the temporal and the spatial frequency of the stimulus, and do not correlate well with image speed. Higgins (2004) proposed a non-directional motion unit with features that are consistent with behavioral experiments based on the use of image speed by honeybees (Srinivasan and Zhang, 1993; Srinivasan *et al.*, 1996, 2000). This unit is based on the multiplication of a high-pass filtered photoreceptor signal with delayed (low-pass filtered) signals from two adjacent photoreceptors (also high-pass filtered), as shown in Figure 7.1a. In this chapter we show that if the multiplication operation is replaced with a sum, the amplitude of the resulting signal encodes speed information that is also consistent with the biological data. This proposed unit, shown in Figure 7.1b, is closely related to the transmedullary cell Tm1 as implemented in the one-dimensional version of the neuronally-based EMD model (refer to Fig. 2.2).

## 7.1   Background and Previous work

Higgins (2004) presented results that showed that the mean response of the non-directional motion unit in Figure 7.1a (which we will call ND-M) is roughly proportional to speed and independent of spatial frequency for a range of speeds and spatial frequencies. This result is illustrated in Figure 7.2. The roughly parallel lines in the contour plot in Figure 7.2a suggest a weak dependence of the ND-M speed tuning on spatial frequency over a range. Figure 7.2b shows that the mean responses of ND-M at various spatial frequencies are roughly proportional to the stimulus speed until the peak response is reached. Moreover, in agreement with the results of behavioral experiments with honeybees (Srinivasan and Zhang, 1993), the mean response of ND-M to sinusoidal counterphase flicker stimulation is weaker than that to sinusoidal motion stimulation (Higgins, 2004). In order to explain how honeybees could use the speed information in ND-M, Higgins proposed a model in which an array of ND-M units for each compound eye of the insect are summed over space and the resulting signals (for each eye) are subtracted from each other.

In this chapter we show that the amplitude of the unit shown in Figure 7.1b (which we will call ND-S) has the same type of features as the mean response of ND-M. While both units are inspired by electrophysiological results from the transmedullary-cell Tm1 (see Discussion), ND-S is closely related to the Tm1 unit in the neuronally-based EMD model.

## 7.2   Methods

To derive mathematical expressions for the amplitude of the response of the ND-S unit in Figure 7.1b to sinusoidal motion stimulation and stimulation with sinusoidal counterphase flicker, we used the following formulae. The moving stimulus was a one-dimensional sinusoidal grating

$$S(t,x) = \frac{1}{2} \cdot (1 + C \cdot sin(\omega_t \cdot t + \omega_x \cdot x)) \tag{7.1}$$

where $C$ is the contrast, $\omega_t$ the temporal frequency, and $\omega_x$ the spatial frequency.
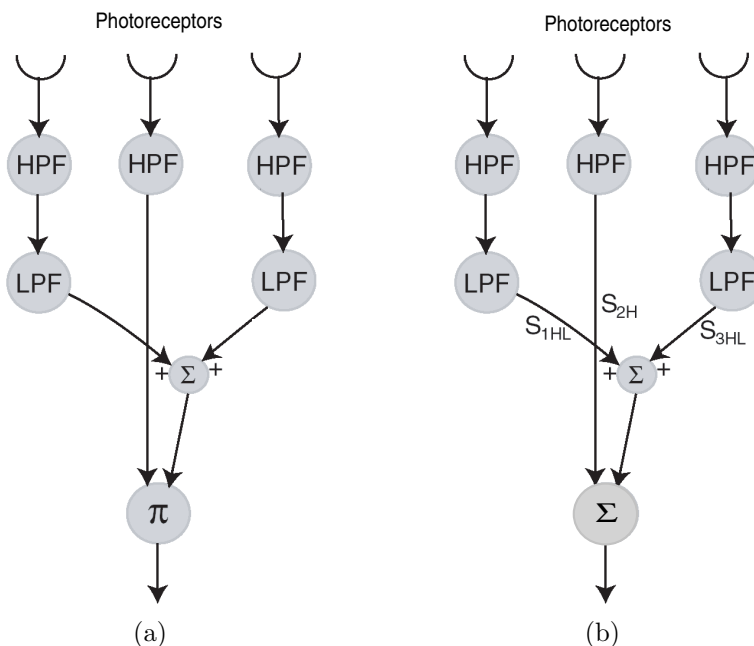
FIGURE 7.1. ND-M and ND-S units. (a) The non-directional motion unit proposed by Higgins (2004), which we refer to as ND-M. (b) The ND-S unit produced by replacing the multiplication ($\prod$) operation in ND-M by a sum ($\sum$).
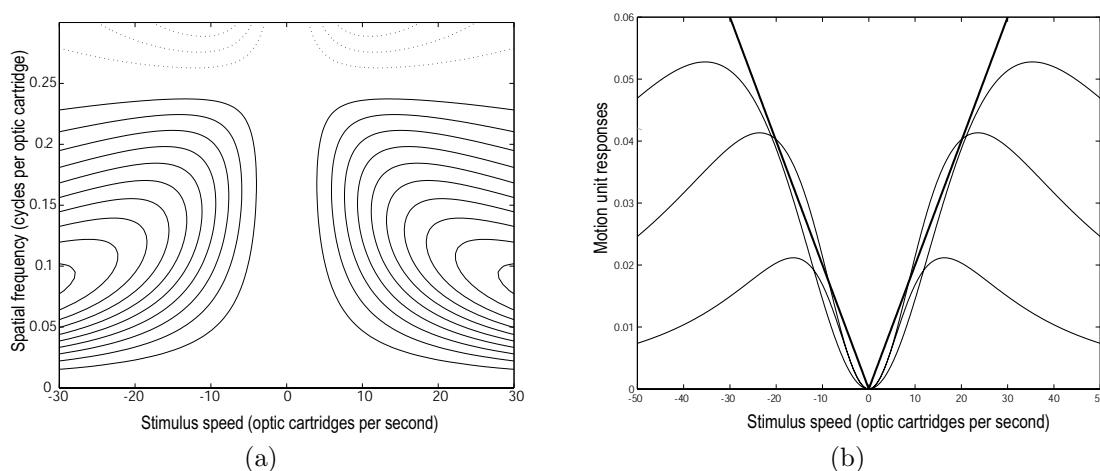


FIGURE 7.2. Mean ND-M responses. (a) Contour plot of the mean ND-M response as stimulus speed and spatial frequency are varied. Contour lines were drawn every 0.005 response units. Contours of positive responses are drawn with solid lines and contours of negative responses are drawn with dotted lines. Contour lines roughly parallel to the spatial frequency axis indicate speed tuning that is relatively insensitive to spatial frequency. (b) Speed tuning of mean ND-M response as spatial frequency is varied. Bold lines show a constant multiple of absolute speed. The speed tuning of the mean ND-M response roughly follows the line of constant speed until the peak. The spatial frequencies used were (from largest to smallest response) 0.09, 0.14, and 0.20 cycles per optic cartridge.

The sinusoidal counterphase (reversing contrast) flickering stimulus was

$$S_c(t, x) = \frac{1}{2}(1 + C \cdot sin(\omega_f \cdot t) \cdot sin(\omega_x \cdot x)) \tag{7.2}$$

where $\omega_f$ is the frequency of the contrast reversals.

In order to make our results comparable to the results presented in Higgins (2004), we allowed, without loss of generality, the spacing between adjacent photoreceptors $\triangle$ to be one, which resulted in the relative phase between sinusoidal inputs to neighboring photoreceptors $\phi_x = \omega_x$. The time-constant of all filters $\tau$ was set to 50 ms. As in Higgins (2004), the expression for the first-order high-pass filter magnitude response $h_1$ was:

$$h_1(\omega_t) = \frac{\omega_t \cdot \tau}{\sqrt{1 + (\omega_t \cdot \tau)^2}} \tag{7.3}$$

The magnitude response $h_2$ and the phase response $\phi_2$ of the low-pass filter were

$$h_1(\omega_t) = \frac{1}{\sqrt{1 + (\omega_t \cdot \tau)^2}} \tag{7.4}$$

and

$$\phi_2(\omega_t) = -tan^{-1}(\omega_t \cdot \tau) \tag{7.5}$$

The stimulus speed $v$ was computed as the ratio of the stimulus temporal and spatial frequencies ($v = \frac{\omega_t}{\omega_x}$). Only spatial frequencies below 0.3 cycles per optic cartridge were considered, as frequencies above this range are extremely attenuated by the insect optics (Snyder, 1979).

In addition to direct evaluations of the mathematical expression for the amplitude of the ND-S unit, we present (in Figure 7.4) the results of the spatial summation of the rectified responses of a simulated array of ND-S units. The responses of the ND-S units were rectified by taking the absolute value. The simulations incorporated a 100-pixel image viewed by 50 equally spaced photoreceptors and the same number of ND-S units.

## 7.3   Results

In response to the moving sinusoidal stimulus in Equation 7.1, the signals $S_{1HL}$, $S_{2H}$, and $S_{3HL}$ in Figure 7.1b can be expressed as (see Methods for definitions):

$$S_{1HL} = \frac{C}{2} \cdot h_1 \cdot h_2 \cdot sin(\omega_t \cdot t + \phi_1 + \phi_2) \tag{7.6}$$

$$S_{2H} = \frac{C}{2} \cdot h_1 \cdot sin(\omega_t \cdot t + \phi_1 + \phi_x) \tag{7.7}$$

$$S_{3HL} = \frac{C}{2} \cdot h_1 \cdot h_2 \cdot sin(\omega_t \cdot t + \phi_1 + \phi_2 + 2\phi_x) \tag{7.8}$$

where for simplicity we assume that the absolute phase of the stimulus relative the leftmost photoreceptor in Figure 7.1b is zero. The amplitude of the ND-S unit, computed by adding the three signals, can be shown to be

$$A_{ND-S} = \frac{C}{2} \cdot h_1 \cdot \sqrt{4h_2 \cdot [h_2 \cdot cos^2(\phi_x) + cos(\phi_x) \cdot cos(\phi_2)] + 1} \tag{7.9}$$

Substituting the expressions of the filter magnitude and phase response and using the fact that $\phi_x = \omega_x$ results in

$$A_{ND-S} = \frac{C}{2} \cdot \frac{\omega_t \cdot \tau}{1 + (\omega_t \cdot \tau)^2} \cdot \sqrt{4[\cdot cos^2(\omega_x) + cos(\omega_x)] + (\omega_t \cdot \tau)^2 + 1} \tag{7.10}$$
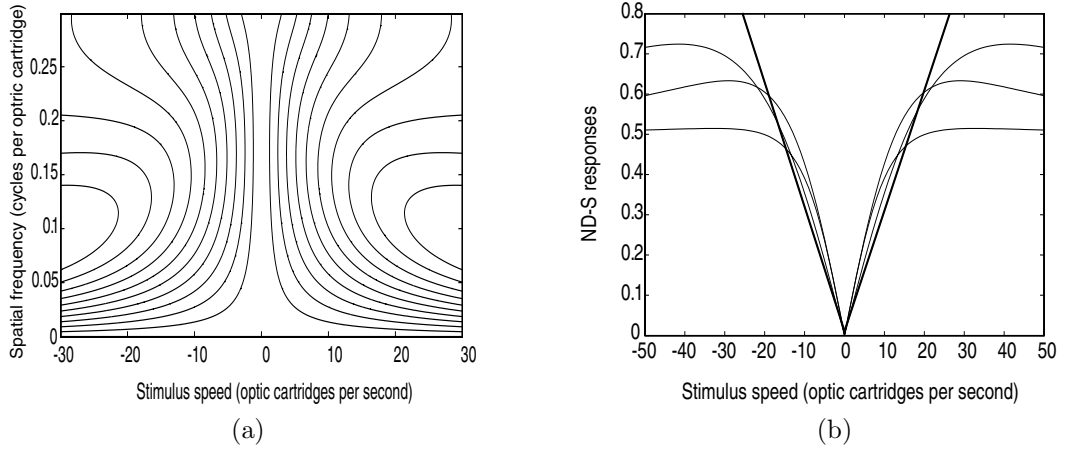
FIGURE 7.3. Amplitude of ND-S responses. (a) Contour plot of the amplitude of the ND-S responses ($A_{ND-S}$) as the stimulus speed and spatial frequency are varied. Ten contour lines were drawn at equally spaced response levels. Contour lines roughly parallel to the spatial frequency axis indicate speed tuning that is relatively insensitive to spatial frequency. (b) Speed tuning of $A_{ND-S}$ as the spatial frequency is varied. Bold lines show a constant multiple of absolute speed. The $A_{ND-S}$ responses roughly follow the line of constant speed until the peak. The spatial frequencies were (from largest to smallest response) 0.09, 0.14, and 0.20 cycles per optic cartridge. Notice that the shape of the responses (including the peak values) are relatively insensitive to the spatial frequency. Compare to Figure 7.2.

Figure 7.3a shows the contour plot of this response. Notice that at speeds below ten optic cartridges per second, the contour lines are nearly parallel to the spatial frequency axis. This insensitivity of the speed tuning to spatial frequency covers most of the spatial frequency range, including lower and higher spatial frequencies than the ND-M contour lines in Fig. 7.2a. As the speed increases, the range in which the contour lines are roughly parallel to the spatial frequency axis becomes more restricted, in a similar manner to the ND-M contour lines.

The rough insensitivity of the $A_{ND-S}$ speed tuning to spatial frequency translates into responses at various spatial frequencies that are proportional to speed over a range. Figure 7.3b shows the speed tuning of $A_{ND-S}$ for three spatial frequencies. The traces roughly follow the line of constant speed in a similar manner to the ND-M mean responses in Figure 7.2b. Notice that the peak values and shapes of the ND-S response amplitudes at the three spatial frequencies are more similar than the ND-M mean responses at the same frequencies, reflecting a higher degree of insensitivity to spatial frequency.

In order to compare the amplitude of the response of ND-S to motion with the amplitude of its response to a counterphase flicker, we derive an expression for the ND-S response amplitude when the stimulus is the sinusoidal reversing-contrast flicker given in Equation 7.2. When responding to this stimulus, the signals $S_{1HL}$, $S_{2H}$, and $S_{3HL}$ in Figure 7.1b can be expressed as (see Methods for definitions):

$$S_{1HL} = \frac{C}{2} \cdot h_1 \cdot h_2 \cdot sin(\omega_f \cdot t + \phi_1 + \phi_2) \cdot sin(\omega_x \cdot p_0) \tag{7.11}$$

$$S_{2H} = \frac{C}{2} \cdot h_1 \cdot sin(\omega_f \cdot t + \phi_1) \cdot sin(\omega_x(p_0 + 1)) \tag{7.12}$$

$$S_{3HL} = \frac{C}{2} \cdot h_1 \cdot h_2 \cdot sin(\omega_f \cdot t + \phi_1 + \phi_2) \cdot sin(\omega_x(p_0 + 2)) \tag{7.13}$$

where $p_0$ is the spatial position of the leftmost photoreceptor in Figure 7.1b with respect to the flickering sinusoidal grating. By summing the three signals and using common trigonometric identities, the amplitude of ND-S to the counterphase stimulus can be expressed as

$$A_{ND-S_c} = \frac{C}{2} \cdot h_1 \cdot sin(\omega_x(p_0 + 1)) \cdot \sqrt{4h_2 \cdot [h_2 \cdot cos^2(\phi_x) + cos(\phi_x) \cdot cos(\phi_2)] + 1} \qquad (7.14)$$

Comparing Equations 7.14 and 7.9, the amplitude of the Tm1 response to the counterphase flicker is the amplitude of its response to motion at the same frequency multiplied by $sin(\omega_x(p_0 + 1))$. Thus, depending on the spatial position of the Tm1 unit with respect to the flickering grating the amplitude of the Tm1 response to counterphase flicker can be at most equal to the Tm1 response to motion, and it is on average weaker.

Unlike ND-M, the mean value of the ND-S response is always zero. One could argue that the mean level of a signal may be easier to process by postsynaptic neuronal processes than the amplitude of modulations centered at zero from a signal such as ND-S. One way in which the information in the amplitude of ND-S can be extracted into the mean response of a signal is if the ND-S output is rectified and then smoothed by a low-pass filter. Figure 7.4a shows a sample response of a signal computed as the spatial sum of the rectified outputs of an array of ND-S units (see Methods). Summing the outputs over space had the effect of removing the traces of the oscillatory components from the response, so smoothing by a low-pass filter was not necessary. Figure 7.4b shows the speed tuning of the mean value of the signal at three spatial frequencies for a moving sinusoidal stimulus and for a sinusoidal counterphase flickering stimulus. As predicted by Equation 7.14, the responses to the counterphase flicker are weaker than the responses to motion. Notice that both types of stimuli produce responses that follow lines of constant speed, but in the case of flicker, the speeds predicted by the responses are lower than those predicted in the case of motion.

## 7.4  Discussion

In 1995, Douglass and Strausfeld presented electrophysiological recordings from the transmedullary cell Tm1, showing the response of the cell to a moving stimulus and to wide-field square-wave flicker. In response to motion, Tm1 showed modulations at frequencies which in one direction of stimulation matched the temporal frequency of the stimulus, and in the opposite direction exhibited what appeared to be a weak frequency doubling. This apparent frequency doubling in the Tm1 response may be produced if the inputs to Tm1 (T1 and L2) are multiplied. This, however, produces modulations at twice the temporal frequency of the stimulus for both directions of stimulation. Similarly, if the inputs to Tm1 are summed, as assumed in the neuronally-based EMD model, the modulations in the response match the temporal frequency of the stimulus for both directions of stimulation. Thus, the Tm1 recordings appear to support the computation of Tm1 as a sum of its inputs when the stimulus moves in one direction, and the computation of Tm1 as the multiplication of its inputs when the stimulus moves in the other direction.

The apparent frequency doubling in the Tm1 electrophysiology was an inspiration for the ND-M unit proposed by Higgins (2004). Replacing the high-pass filters by relaxed high-pass filters in the low-pass filtered pathways, and inverting all the inputs to the multiplication stage, would indeed make ND-M equivalent to a Tm1 unit that is computed by the multiplication of L2 and T1 in a one-dimensional EMD model (refer to Fig. 2.2). Computing Tm1 in this manner, however, produces results that are not consistent with other behavioral and electrophysiological results available. If the photoreceptor signals from T1 and L2 are multiplied, the resulting output produces only positive responses to wide-field square-wave flicker stimulation. This contradicts Tm1 electrophysiology which shows positive responses relative the resting potential when the luminance level drops (light turns off), and negative responses when the luminance level rises (light turns on). Furthermore, the response of a unit that multiplies its inputs is zero if any of the inputs are zero. In the previous
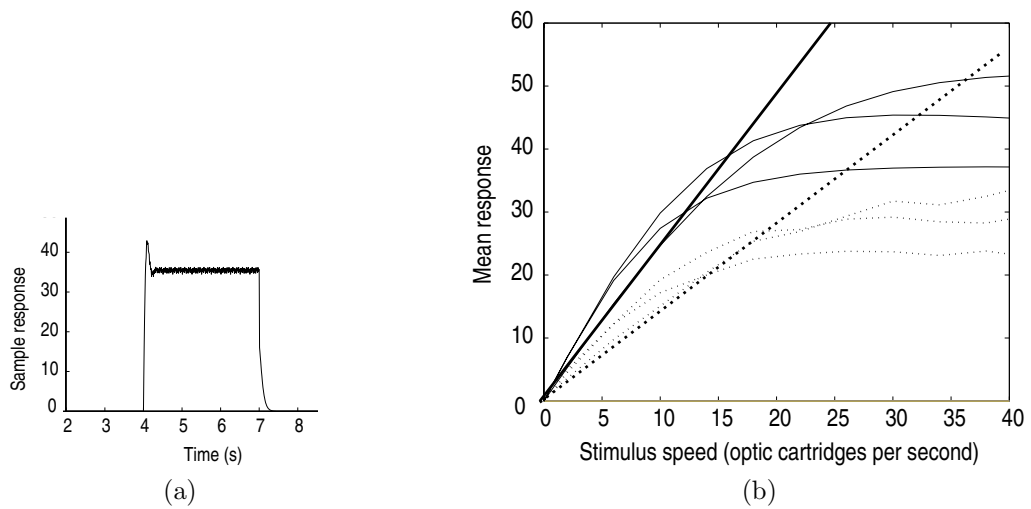
FIGURE 7.4. Spatial sum of the rectified outputs of an array of ND-S units. (a) Sample response produced when summing over space the rectified ND-S responses to a moving stimulus with speed equal to 20 optic cartridges per second (spatial frequency is 0.2 cycles per optic cartridges). (b) Speed tuning of the mean response produced after the spatial sum. Solid lines represent the speed responses when the stimulus was a moving sinusoidal grating while the dotted traces were produced when the stimulus was a sinusoidal counterphase flickering grating. The spatial frequencies were (from largest to smallest response) 0.09, 0.14, and 0.20 cycles per optic cartridge. Bold solid and dotted lines are constant multiples of speed. Note the speed responses produced with counterphase flicker are weaker than those produced with motion stimulation.

chapter, however, we learned that genetically deleting L2 or T1 does not result into a complete impairment of the fly's response to motion, but rather into a reduction in the magnitude of the response. Even if the multiplication at Tm1 is implemented as shunting inhibition, the predictions from the resulting model would still be in disagreement with the outcome of the genetic experiments.

Because both the behavioral results in Chapter 6 and the Tm1 response to flicker from the electrophysiology can be explained if the inputs to Tm1 are summed, modeling Tm1 in this manner appears to be a better alternative. Furthermore, the results we presented in this chapter show that speed information that can be obtained by the mean response of ND-M is encoded in the amplitude of ND-S. Other simulations (not shown) show that our results are still valid if ND-S is replaced by Tm1 in the neuronally-based EMD model of Figure 2.2, which has two relaxed high-pass filters and all inputs inverted. Future work in this area includes investigating other ways in which the Tm1 inputs could be combined (see Chapter 8).

# Final Comments and Future Work

We have presented a computational exploration of various aspects of fly motion detection, including contrast and stimulus size saturation (Chapter 3) and adaptation (Chapters 4 and 5). Within the topic of adaptation, we have proposed, for the first time, a neuronal mechanism that may explain the contrast gain reduction measured in tangential cell electrophysiology (Chapter 4) and we have showed that we can predict results previously explained in terms of EMD filter adaptation with an EMD model with static filter parameters (Chapter 5). Our expanded model for elementary motion detection is supported by tangential cell electrophysiology and behavioral experiments with genetically-altered flies (Chapter 6). In addition, we have identified a possible mechanism through which insects could extract speed information from the projected retinal image (Chapter 7).

The principles of neural computation in the fly visual motion system may be applied in the design of engineering devices that require the extraction of motion and speed information from a visual image. Such devices may be used for navigation in applications such as autonomous robots or unmanned vehicles. A system which computes the apparent image speed of the visual stimulus, as projected into the "eye" or visual sensor may be used for the computation of depth by parallax, where movements of the eye result in apparent motion of the objects observed, with relative speeds that are in proportion to their relative depths. When calibrated, such a system could be used to estimate the distance to obstacles or targets.

One of the challenges of extracting velocity information from a visual stimulus is that the responses of motion detectors depend not only on the speed of the stimulus, but also on other stimulus parameters such as contrast, pattern size and spatial frequency. Incorporating contrast and pattern size saturation (see Chapter 3) removes the dependence of the system on these parameters over a range, and if the threshold for saturation is sufficiently low, this range may include most stimuli the system would encounter in the real world. Contrast saturation, however, appears to be accompanied by a loss of sensitivity to fluctuations of the stimulus speed. Contrast gain reduction (see Chapter 4), a mechanism which gradually reduces the gain of the system, may help to bring the response level below the saturation threshold. Thus, by gradually reducing the response to sustained stimulation (which presumably has already been neuronally processed), the sensitivity to new stimuli is at least partially restored.

Interestingly, experiments with honeybees suggest that speed information may be provided not from the output of a directionally-selective motion detector, but from a separate non-directional system. The transmedullary cell Tm1 in the neuronally-based model appears to already encode in its amplitude speed information independent of the stimulus spatial frequency (see Chapter 7). The simplicity of the computation incorporated at the Tm1 unit may be suggestive of an architecture where relatively simple individual units may accomplish complex tasks, when a massive array of such units operates in parallel. The world of engineering and computer science, vastly dominated by sequential processing, may be inspired by such architectures, which result not only in more elegant designs, but also in more reliable, and potentially much faster information processing.

Undeniably, one of the most remarkable qualities of biological systems is robustness. Redundancies in the neural pathways protect the insects against damage and defects in the neural architecture, and are features favored by evolution. The motion detection system which is at the core of a number of important insect behaviors is probably not the exception. The neuronally-based EMD model incorporates redundant input pathways (see Chapter 6), which may help ensure that stimulus information is reliably available for the computation of motion. Such a design architecture would provide clear benefits to an engineering system operating in unpredictable environments.

## 8.1 Future Work

A number of questions arising from our work remained to be answered. Contrast saturation, which we conveniently modeled by inserting a saturating nonlinearity into individual pathways in the neuronally-based EMD model, is likely a much more complicated feature than our simplistic approach assumes. As discussed in Chapter 3, using a sigmoid function to produce saturation fails to account for some features of the tangential cell electrophysiology. Better results may be obtain if the sigmoid is not centered at zero but at the sustained component of the input signal. It is possible that the reduction in the afterimage oscillations in the tangential cell step response when the contrast is increased (refer to Figure 5.4a), could be explained by a more biologically accurate model of contrast saturation. At the least, such a possibility ought to be ruled out before evaluating other options like adaptation of the time constant of the EMD filters.

In this thesis we discussed contrast saturation (Chapter 3) and contrast gain reduction (Chapter 4) as two separate features. It is indeed possible that they are caused by the same synaptic mechanism. Suggestive of this is the fact that our results indicate that they occur in the same or in very close locations in the EMD pathways (contrast gain reduction was proposed to occur on the Tm1 synapses onto T5 and Tm9, while contrast saturation was said to occur in the Tm1 and Tm9 synapses onto T5). More work is required to evaluate whether this could be the case.

The implementation of the model for contrast gain reduction we presented in Chapter 4 was aimed at comparing our results with the responses of tangential cells to stimulation with sinusoidal or square-wave gratings. It would be very desirable to compare the model responses to tangential cell recordings using more complex or realistic types of stimuli. While the implementation of the model would have to be adjusted, the principles behind it should still hold regardless of the complexity of the stimulus. Unfortunately, very few examples of LPTC responses to realistic stimuli are available at the time of this work.

While the responses of the model LPTC to stimuli moving at high temporal frequencies were comparable to H1 electrophysiology (refer to Fig. 4.6), the response of the model to a stimulus moving at 20 Hz was weaker than the response of an HS cell to the same stimulus (compare Figures 4.10 and 4.1). Future work may include exploring possible ways to broaden the temporal frequency tuning of the model. One such possibility could be to incorporate two parallel EMDs, one tuned to low frequencies and the other one tuned to high frequencies, as suggested by O'Carroll (2001).

Finally, as discussed in Chapter 4, if the Tm1 synapses are the site of synaptic depression, then the response of Tm1 to wide-field (sinusoidally modulated) flicker should be significantly weaker than its response to moving sinusoidal gratings. It is possible that amacrine cells implement lateral inhibition, and it is conceivable that such interactions could emphasize the Tm1 response to motion over flicker. Such a possibility is worth considering in future work. If it is determined that Tm1 could not be responsible for contrast gain reduction, then other possibilities could be examined, such as the non-directional T4 bushy T-cell which is not currently incorporated in the neuronally-based EMD model.

# References

Abbott, L.F, K. Sen, J.A. Varela, and S.B. Nelson (1997). Synaptic depression and cortical gain control. *Science* 275: 220–224.

Barlow, H. B. and W. R. Levick (1965). The mechanism of directionally selective units in rabbit's retina. *J. Physiol. (Lond.)* 178: 477–504.

Bausenwein, B. and K.-F. Fischbach (1992). Separation of functional pathways in the fly's medulla: Combination of 2-deoxyglucose studies with anatomical fine analysis. In Singh, R. N., editor, *Nervous Systems: Principles of design and function*, pp. 223–239. Wiley Eastern, New Delhi.

Beersma, D.G.M., D.G. Stavenga, and J.W. Kuiper (1977). Retinal lattice, visual field, and binocularities in flies. *J. Comp. Physiology* 119: 207–220.

Bex, P.J., S. Bedingham, and S.T. Hammett (1999). Apparent speed and speed sensitivity during adaptation to motion. *J. Opt. Soc. Amer. A* 16: 2817–2824.

Borst, A. and M. Dickinson (2003). Visual course control in flies. In *The handbook of brain theory and neural networks*, pp. 1205–1210. Bradford Books/MIT Press, USA.

Borst, A. and M. Egelhaaf (1987). Temporal modulation of luminance adapts time constant of fly movement detectors. *Biological Cybernetics* 56: 209–215.

Borst, A., M. Egelhaaf, and J. Haag (1995). Mechanisms of dendritic integration underlying gain control in fly motion-sensitive interneurons. *J. Computational Neuroscience* 2: 5–18.

Borst, A., M. Egelhaaf, and J. Haag (1997). Dendritic computation of direction selectivity and gain control in visual interneuorons. *J. Neuroscience* 17: 6023–6030.

Borst, A. and J. Haag (2002). Neural networks in the cockpit of the fly. *J. Comp. Physiology A* 188: 419–437.

Borst, A., C. Reisenman, and J. Haag (2003). Adaptation of response transients in fly motion vision. II: Model studies. *Visual Neuroscience* 43: 1309–1322.

Braitenburg, V. and F.C. Taddei (1966). Landing reaction of *Musca Domestica* induced by visual stimuli 53: 155.

Buchner, E. and S Buchner (1984). Neuroanatomical mapping of visually induced neuron activity in insects by 3H-deoxyglucose. In Ali, M. A., editor, *Photoreception and vision in invertebrates*, pp. 623–634. Plenum Press, New York.

Burton, B.G. (2000). Problems and solutions in early visual processing. In Baddeley, R., P. Hancock, and Födiák P., editors, *Information Theory and the Brain*, pp. 253–271. Cambridge University Press.

Buschbeck, E. K. and N. J. Strausfeld (1996). Visual motion-detection circuits in flies: small field retinotopic elements responding to motion are evolutionarily conserved across taxa. *J. Neurosci.* 16: 4563–4578.

Campos-Ortega, J. and N. J. Strausfeld (1973). Synaptic connections of intrinsic cells and basket arborizations in the external plexiform layer of the fly's eye. *brain* 59: 119–136.

Chance, F.S., S.B. Nelson, and L.F. Abbott (1998). Synaptic depression and the temporal response characteristics of v1 cells. *Trans Roy Soc Lond B* 18: 4785–4799.

Clifford, C.W.G., M.R. Ibbotson, and K. Langley (1997). An adaptive Reichardt detector model of motion adaptation in insects and mammals. *Visual Neuroscience* 4: 741–749.

Clifford, C.W.G. and K. Langley (1996). Psychophysics of motion adaptation parallel insect electrophysiology. *Curr. Biol.* 6: 1340–1342.

Collett, T.S. and M.F. Land (1978). How hoverflies compute interception courses. *J. Comp. Physiology* 125: 191–204.

Coombe, P. E., M. V. Srinivasan, and R. G. Guy (1989). Are the large monopolar cells of the insect lamina on the optomotor pathway? *J. Comp. Physiology A* 166: 23–35.

Coombe, P.E. and M Heisenberg (1986). The structural brain mutant *Vacuolar medulla* of *Drosophila Melanogaster* with specific behavioral defects and cell degeneration in the adult. *J. Neurogenet* 3: 135–158.

de Ruyter van Steveninck, R. R., W.H. Zaagman, and H.A.K. Mastebroek (1986). Adaptation of transient responses of a movement sensitive neuron in the visual system of the blowfly *Calliphora erythrocephala*. *Biological Cybernetics* 54: 223–236.

Douglass, J. K. and N. J. Strausfeld (1995). Visual motion detection circuits in flies: Peripheral motion computation by identified small field retinotopic neurons. *J. Neurosci.* 15: 5596–5611.

Douglass, J. K. and N. J. Strausfeld (2004). Sign-conserving amacrines in the fly's external plexiform layer. In Review, Visual Neuroscience.

Dvorak, D., M. V. Srinivasan, and A. S. French (1979). The contrast sensitivity of fly movement-detecting neurons. *Vision Research* 20: 397–407.

Eckert, H. and D.R. Dvorak (1983). The centrifugal horizontal cells in the lobula plate of the blowfly phaenicia sericata. *J. Insect Physiology* 29: 547–560.

Egelhaaf, M. and A. Borst (1989). Transient and steady-state response properties of movement detectors. *J. Opt. Soc. Amer. A* 6: 116–127.

Egelhaaf, M., A. Borst, and W. Reichardt (1989). Computational structure of a biological motion-detection system as revealed by local detector analysis in the fly's nervous system. *J. Opt. Soc. Amer. A* 6: 1070–1087.

Egelhaaf, M., K. Hausen, W. Reichardt, and C. Wehrhahn (1988). Visual course control in flies relies on neuronal computation of object and background motion. *Trends in Neuroscience* 11: 351–358.

Feng, J. (2003). *Computational Neuroscience: A Comprehensive Approach*. Chapman & Hall / CRC Press.

Fetchko, M.J. (2002). Molecular genetic analysis of drosophila eye development: Investigation of a leucine-rich repeat protein's role in cell-cell communication. Ph.D. diss., Pennsylvania State University.

Franceschini, N, N Riehle, and A. Le Nestour (1989). Directionally selective motion detection by insect neurons. In Stavenga, D. G. and R. C. Hardie, editors, *Facets of Vision*, pp. 360–390. Springer, Berlin, Heidelberg.

Gabriel, B. (2004). Walking and vision in blowflies. Ph.D. diss., University of Groningen.

Georgeson, M.A. and G.D. Sullivan (1975). Contrast constancy: deblurring in human vision by spatial frequency channels. *J. Physiology* 3: 627–656.

Gronenberg, W. and N. J. Strausfeld (1991). Descending pathways connecting the male-specific visual system of flies to the neck and flight motor. *Journal of Comparative Physiology A* 169: 413–426.

Harris, R. A., D. C. O'Carroll, and S. B. Laughlin (1999). Adaptation and the temporal delay filter of fly motion detectors. *Vision Research* 39: 2603–2613.

Harris, R.A. and D.C. O'Carroll (2002). Afterimages in fly motion vision. *Visual Neuroscience* 42: 1701–1714.

Harris, R.A., D.C. O'Carroll, and S.B. Laughlin (2000). Contrast gain reduction in fly motion adaptation. *Neuron* 28: 595–606.

Harrison, R.R. and C. Koch (1999). An analog VLSI implementation of a visual interneuron: enhanced sensory processing through biophysical modeling. *Int. J. of Neural Systems* 5: 391–395.

Hassenstein, B. and W. Reichardt (1956). Systemtheorische analyse der Zeit-, Reihenfolgen- und Vorzeichenauswertung bei der Bewegungsperzeption des Rüsselkäfers Chlorophanus. *Zeitschrift für Naturforschung* 11b: 513–524.

Hausen, K. (1982). Motion sensitive interneurons in the optomotor system of the fly. I. The horizontal cells: structure and signals. *Biological Cybernetics* 45: 143–156.

Hausen, K. (1984). The lobula-complex of the fly: structure, function, and significance in visual behaviour. In Ali, M.A., editor, *Photoreception and vision in invertebrates*, pp. 523–599. Plenum Press.

Hengstenberg, R. (1983). Common visual response properties of giant vertical cells in the lobula plate of the blowfly calliphora. *J. Comp. Physiology A* 149: 179–193.

Hengstenberg, R. (1993). Multisensory control in insect oculomotor systems. *Rev Oculomot Res* 5: 285–298.

Higgins, C.M. (2004). Non-directional motion may underlie insect behavioural use of image speed. *Biological Cybernetics* 91: 326–332.

Higgins, C.M., J.K. Douglass, and N.J. Strausfeld (2004). The computational basis of an identified neuronal circuit for elementary motion detection in dipterous insects. *Visual Neuroscience* 21: 567–586.

Ibbotson, M.R., C.W.G. Clifford, and R.F. Mark (1998). Adaptation to visual motion in directional neurons of the nucleus of the optic tract. *J. Neurophysiology* 79: 1481–14.

Keller, A. (2002). Genetic intervention in sensory systems of the fly. Ph.D. diss., Bayerischen Julius-Maximilians-Universität Würz-burg.

Kirchner, W.H. and M.V. Srinivasan (1989). Freely flying honeybees use image motion to estimate object distance 76: 281–282.

Koch, C. (1999). *Biophysics of computation: information processing in single neurons*. Oxford University Press, New York, NY.

Krapp, H. G., B. Hengstenberg, and R. Hengstenberg (1998). Dendritic structure and receptive-field organization of optic flow processing interneurons in the fly. *J. Neurophysiology* 79: 1902–1917.

Land, M.F. (1992). Visual tracking and pursuit:humans and arthropods compared. *J. Insect Physiology* 38: 939–951.

Land, M.F. and T.S. Collett (1974). Chasing behavior of house flies (*Fannia canicularis*). *J. Comp. Physiology* 89: 331–357.

Land, M.F. and H. Eckert (1985). Maps of the acute zones of fly eyes. *J. Comp. Physiology A* 156: 525–538.

Lehrer, M. and M.V. Srinivasan (1992). Freely flying bees discriminate between stationary and moving objects: performance and possible mechanisms. *J. Comp. Physiology A* 171: 457–467.

Maddess, T. (1986). Afterimage-like effects in the motion sensitive neuron H1. *Trans Roy Soc Lond B* 228: 433–459.

Maddess, T. and S.B. Laughlin (1985). Adaptation of the motion-sensitive neuron H1 is generated locally and governed by contrast frequency. *Trans Roy Soc Lond B* 225: 251–275.

Melano, T. and C. M. Higgins (2005). The neuronal basis of direction selectivity in lobula plate tangential cells. *Neurocomputing* 65-66C: 153–159.

Neher, E. (1998). Vesicle pools and ca2+ domains: New tools for understanding their roles in neurotransmitter release. *Neuron* 20: 389–399.

Nishikawa, K.C. (2002). Evolutionary convergence in nervous systems: Insights from comparative phylogenetic studies. *Brain Behavior and Evolution* 59: 240249.

O'Carroll, D. C. (2001). Motion adaptation and evidence for parallel processing in the lobula plate of the bee-fly bombylius major. In Zanker, J. M. and J. Zeil, editors, *Motion Vision: computational, neural, and ecological constraints*, pp. 381–394. Springer Verlag.

Olberg, R.M., A.H. Worthington, and K.R. Venator (2000). Prey pursuit and interception in dragonflies. *J. Comp. Physiology A* 186: 155–162.

Reisenman, C., J. Haag, and A. Borst (2003). Adaptation of response transients in fly motion vision. I: Experiments. *Visual Neuroscience* 43: 1291–1307.

Rivera-Alvidrez, Z. and C.M. Higgins (2005). Contrast saturation in a neuronally-based model of elementary motion detection. *Neurocomputing* 65-66C: 173–179.

Single, S. and A. Borst (1998). Dendritic integration and its role in computing image velocity. *Science* 281: 1848–1850.

Snakevitch, I. and N. J. Strausfeld (2004). Chemical neuroanatomy of the fly's movement detection pathway. *J. Comp. Neurology* 486: 6–23.

Snyder, A. W. (1979). Physics of vision in compound eyes. In Autrum, H., editor, *Comparative Physiology and evolution of vision in invertebrates: Invertebrate photoreceptors, Volume VII/6A of Handbook of sensory physiology*, chapter 5, pp. 225–313. Springer-Verlag.

Srinivasan, M. V. and S. W. Zhang (1993). Evidence for two distinct movement-detecting mechanisms in insect vision 80: 38–41.

Srinivasan, M. V., S. W. Zhang, J. S. Chahl, E. Barth, and S. Venkatesh (2000). How honeybees make grazing landings on flat surfaces. *Biological Cybernetics* 83: 171–183.

Srinivasan, M. V., S. W. Zhang, M. Lehrer, and T. S. Collett (1996). Honeybee navigation en route to the goal: visual flight control and odometry. *J. Exp. Biol.* 199: 237–244.

Srinivasan, M.V., M. Lehrer, W.H. Kirchner, and S.W. Zhang (1991). Range perception through apparent image speed in freely flying honeybees. *Visual Neuroscience* 6: 519–535.

Strausfeld, N. J. and D. R. Nässel (1980). Neuroarchitectures serving compound eyes of Crustacea and insects. In Autrum, H., editor, *Handbook of Sensory Physiology, VII/68*, pp. 1–132. Springer.

Strausfeld, N.J. (1970). Golgi studies on insects. Part II. The optic lobes of diptera. *Phylos Roy Soc Lond B* 258: 135–223.

Takahashi, M., Y. Kovalchuck, and D. Attwell (1995). Pre- amd postsynaptic determinants of epsc waveform at cerbellar fiber and purkinje cell synapses. *J. Neuroscience* 15: 5693–5707.

Thompson, P. (1981). Velocity after-effects: the effects of adaptation to moving stimuli on the perception of subsequently seen moving stimuli. *Vision Research* 21: 337–345.

Varela, J.A., K. Sen, J. Gibson, J. Forst, L.F Abbott, and S.B. Nelson (1997). A quantitative description of short-term plasticity at excitatory synapses in layer 2/3 of rat primary visual cortex. *J. Neuroscience* 17: 7926–7940.

Wagner, H. (1982). Flow-field variables trigger landing in flies. *Nature* 297: 147–148.

Wagner, H. (1986). Flight performance and visual control of flight of the free-flying housefly (*Musca Domestica*). ii. pursuit of targets. *Trans Roy Soc Lond B* 312: 553–579.

Wolgemuth, A. (1911). On the after-effect of seen motion. *British Journal of Physiology* 1: 1–117.

Yeates, D.K. and B.M. Wiegmann (1999). Congruence and controversy: toward a higher-level phylogeny of diptera. *Annual Review of Entomology* 44: 397–428.